

Validation of water vapor measured by SABER on the TIMED satellite

Pingping Rong^{a,*}, James M. Russell III^a, Benjamin T. Marshall^b, Larry L. Gordley^b,
Martin G. Mlynczak^c, Kaley A. Walker^d

^a Center for Atmospheric Sciences, Hampton University, Hampton, VA, USA

^b GATS, Inc., Newport News, VA, USA

^c NASA Langley Research Center, Hampton, VA, USA

^d Department of Physics, University of Toronto, Toronto, Ontario, Canada



ARTICLE INFO

Keywords:

SABER H₂O
Out-of-band correction
Coincidences
Long-term variability

ABSTRACT

The Sounding of the Atmosphere using Broadband Emission Radiometry (SABER) measured water vapor (H₂O) had errors of unknown origin that were recently identified and corrected. The cause of the errors was determined to be unaccounted for spectral out-of-band (OOB) radiance in the H₂O channel centered at 6.8 μm arising from ozone emission in the 9.6 μm band. The corrected SABER radiance profiles have been used to produce a long-term H₂O data base labeled as version 2.07 (v2.07). Water vapor volume mixing ratio (VMR) vertical profiles are available in the SABER data archive covering the stratosphere and mesosphere extending from near the tropopause at ~100 hPa (~16 km) to the mesopause region at ~0.006 hPa (~83 km), and over the time period from 25 January 2002 to the present day. The random error of the v2.07 product is smaller than 4% at 60 km and below, while above this altitude it rapidly increases to 30% (at 80 km), mainly due to low signal-to-noise. The estimated systematic error of SABER v2.07 H₂O is about 10–20%. Coincidence analysis between SABER v2.07, MLS v4.2, ACE v3.5–3.6, MIPAS ESA reprocessed v6, and SOFIE v1.3 shows overall excellent agreement in the mean profile with the mean difference being within ±10% in most cases. In the stratopause region SABER H₂O tends to be biased high relative to each of the other data sets used for comparisons especially in the SH polar winter where the mean difference reaches 20% or greater. In polar summer above 80 km, SABER H₂O is biased low by ~20% compared to the other measurements. SABER H₂O therefore reflects the polar winter and spring descent very well but in the summer PMC region the enhancement is weaker than expected. SABER H₂O long-term series in the latitude range 50°S–50°N shows close agreement with MLS on a series of pressure levels throughout the stratosphere and mesosphere on inter-annual to decadal time scales. On these time scales also, throughout the years 2002–2005, SABER and MIPAS long-term time series agree well in the equatorial region which serves as an unprecedented validation for this time period. SABER H₂O also captures the “tape recorder” phenomenon in the tropical tropopause region very well.

1. Introduction

In this paper we assess the data quality of water vapor (H₂O) measured throughout the stratosphere and mesosphere (~15–83 km) over a 17 year period (2002–2018) by the Sounding of the Atmosphere using Broadband Emission Radiometry (SABER) instrument aboard the TIMED satellite (Russell et al., 1999; Tansock et al., 2006). Water vapor (H₂O) is the strongest greenhouse gas in earth's atmosphere and plays an indispensable role in the radiative balance. As a result, it will modulate earth climate change if long-term or decadal trends exist in the H₂O abundance (e.g., Solomon et al., 2010). Long-term change has become a

highlighted issue of our time and the emergence of new data sources will better equip the research community to attack this problem.

Water vapor plays important roles on shorter time scales as well. For example, water vapor serves as a key dynamical tracer of transport from the lower thermosphere to the stratosphere triggered by Stratospheric Sudden Warming (SSW) events (e.g., Bailey et al., 2014). Aside from the liquid form of H₂O on the earth surface, which is by far the largest source of atmospheric H₂O, another primary H₂O source region resides in the stratosphere where methane (CH₄) conversion into H₂O occurs with the highest efficiency (Rong et al., 2016). In the mesosphere at ~70 km altitude, photolysis begins to play a significant role as the H₂O chemical

* Corresponding author. 23 E. Tyler street, Hampton, VA, 23668, USA.

E-mail address: ping-ping.rong@hamptonu.edu (P. Rong).

<https://doi.org/10.1016/j.jastp.2019.105099>

Received 1 May 2019; Received in revised form 29 July 2019; Accepted 30 July 2019

Available online 31 July 2019

1364-6826/© 2019 Elsevier Ltd. All rights reserved.

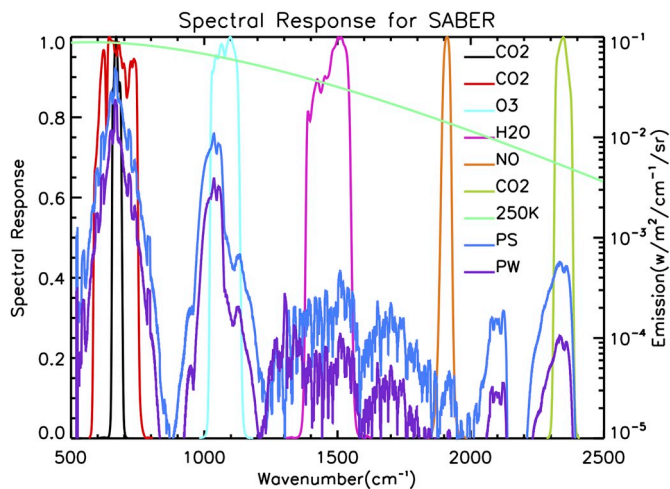


Fig. 1. SABER spectral filter locations and shapes (i.e., smoother curves that reach 1.0 on the left coordinate), a 250 K blackbody emission spectrum (i.e., the broad green curve), and the 50 km tangential height atmospheric limb emission spectra for 280 K (blue) and 250 K (purple), representing polar summer and polar winter respectively. The emission spectra use the scale on the right coordinate. (For interpretation of the references to color in this figure legend, the reader is referred to the Web version of this article.)

lifetime (~1 month) and the transport time scale become comparable (Brasseur and Solomon, 2005).

The H₂O distribution in the polar summer mesosphere is especially worth noting and is of critical importance because the H₂O enhancement in such a relatively high altitude range (e.g., Summers et al., 2001) is not only remarkable, but also it combines with the lowest temperature on Earth in the mesopause region to enable Polar Mesospheric Clouds (PMCs) to form. PMCs also are termed as noctilucent clouds (NLCs) if observed from the ground. PMCs are a magnificent exhibition of H₂O enhancement in the mesosphere and furthermore the increased occurrence of these clouds and their appearance at lower latitudes in recent years has been suggested as a harbinger of global change in the middle atmosphere (Thomas, 2003; Russell et al., 2014). Especially in recent years, a better network of amateur and professional camera settings have resulted in an increasingly better global coverage and therefore an increasing number of reports of lower latitude NLCs. Overall, knowledge of the H₂O global distribution throughout the stratosphere and mesosphere is highly valuable for understanding the respective roles of

atmospheric dynamics and chemistry, and to further address climate change.

The SABER instrument (Russell et al., 1999; Tansock et al., 2006) is a 10-channel broadband infrared limb sounding radiometer (1.27 μm–17 μm) that has been operating nearly continuously aboard the NASA TIMED satellite since it was launched on 7 December 2001. SABER routine data collection began on 25 January 2002 and the products include vertical profiles, with 2 km vertical resolution, of temperature, volume mixing ratios (VMRs) of H₂O (6.8 μm), ozone (O₃) (9.6 μm and 1.27 μm), atomic oxygen ([O]) and hydrogen ([H]), and volume emission rates of nitric oxide (NO) (5.3 μm), hydroxyl (OH) (2.1 μm and 1.6 μm), and excited oxygen (O₂(¹Δ)) (1.28 μm). The measurements extend from the tropopause region to the lower thermosphere, and span latitudes from 53°S to 83°N or 53°N to 83°S daily with alternating latitude coverage every ~60 days that occurs due to spacecraft yaws. The yaws are needed to avoid direct solar radiance from entering the SABER telescope. The experiment, which began its 18th year of data collection on 25 January 2019, is measuring 1,400 profiles of the above

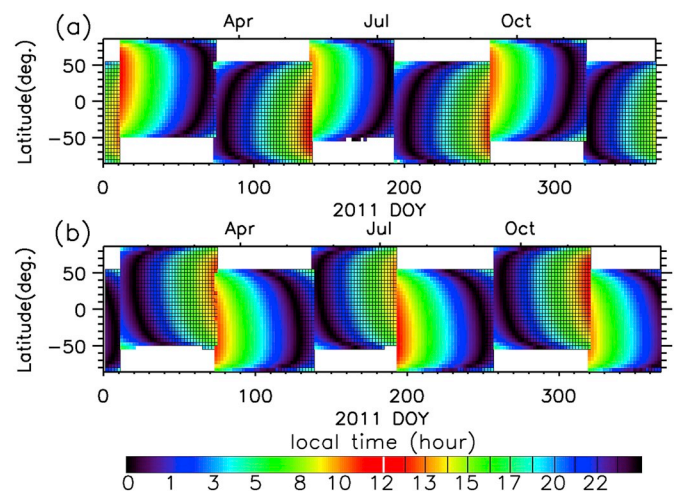


Fig. 2. SABER ascending (a) and descending node (b) local time coverages throughout a year. The alternate north and south polar coverages are due to the yaw effect which refers to the 180° yaw of the space craft roughly every two months. Yaw days are slightly different for each year and the year 2011 is chosen arbitrarily simply because it has the full-year coverage without any missing days. SABER repeats the same local time coverage every two yaw cycles for the ascending or descending node.

Table-1
SABER H₂O Error Estimates in percent.

	Trop ^f	20 km	30 km	40 km	50 km	60 km	70 km	80 km ^e
Systematic Error Sources								
Non-LTE Model	0	0	0	0.5	1	3	7	15
Spectroscopy	1	1	1	1	1	1	1	1
Interfering Gases	2	2	2	1.5	1	0.5	0.5	0.5
Temperature ^a	20	15	12	10	10	12	12	12
Radiance Calibration (1%)	5	3	2.5	2	2.5	3	2.5	2
Registration(50 m)	3	2.5	2	1	2	3	3	3
Total Systematic Error^b (%)	21	16	13	10	11	13	14	20
Random Error Sources								
Measurement Noise	1	1	1	1	1.5	3	10	30
Jitter(20 m)	3	2.5	2	1.5	1.5	1.5	1.5	1.5
Total Random Error^c (%)	3	3	2	2	2	3	10	30
Total Estimated Error^d (%)	21	16	13	11	11	14	18	36

^a Temperature error based on validation results discussed in Remsburg et al. (2008).

^b Total Systematic Error calculated as Root-sum-square (RSS) of individual systematic sources.

^c Total Random Error calculated as RSS of individual random error sources - these errors are reduced by the interleave average procedure.

^d Total Estimated Error is RSS of systematic and random errors and is an upper bound.

^e 80 km estimates are valid for daytime only. Nighttime data at 80 km has very low signal to noise and results are predominately from a-priori climatology.

^f Tropopause.

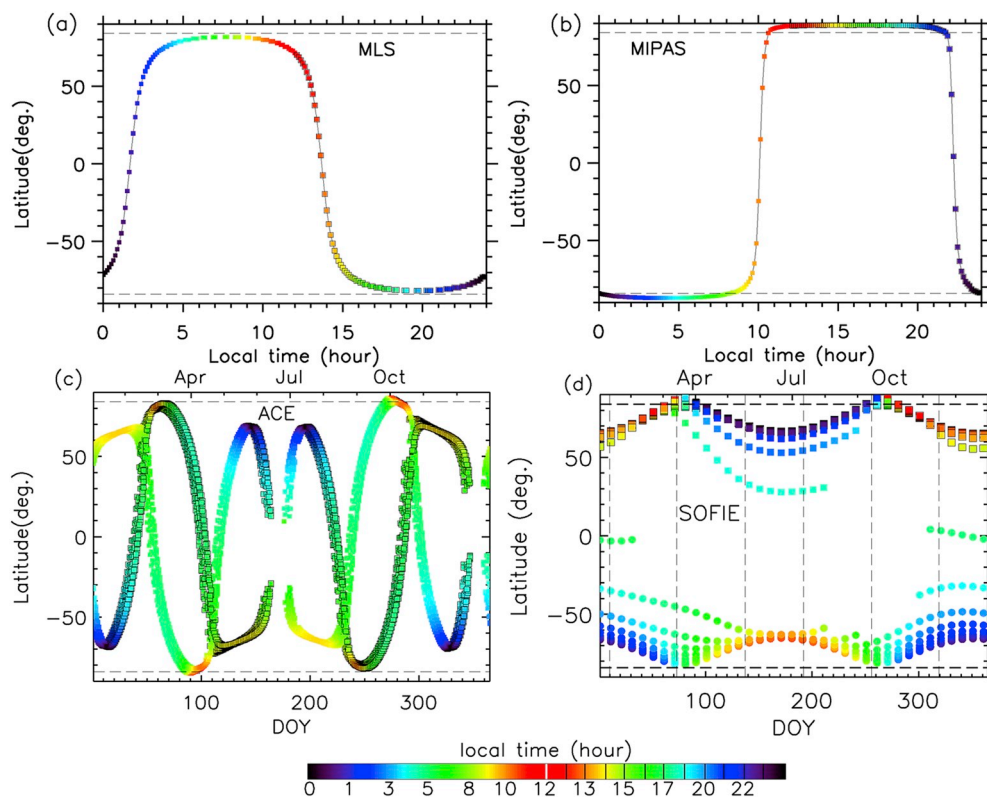


Fig. 3. The local time coverages of the data sets used to validate SABER H₂O. Aura MLS and Envisat MIPAS (a–b) both have repeated local time coverage from day to day. In (a–b) the colors and the horizontal axis provide duplicate information of the local time hours to maintain consistent presentation. Sci-sat1 ACE and AIM SOFIE (c–d) local time coverages vary with day (of year) but roughly repeat themselves from year to year. The ACE coverage shifts slightly over years 2004–2017 while SOFIE migrates toward lower latitudes substantially after 2012. For SOFIE, the dots are for sunrises and the squares are for sunsets. The vertical dashed lines in Fig. 3d mark the SABER 2011 yaw days (see Fig. 2). The horizontal dashed lines in all the panels mark the lowest and highest latitude limits for SABER. (For interpretation of the references to color in this figure legend, the reader is referred to the Web version of this article.)

parameters each day, and the data are widely used throughout the research community.

SABER H₂O is retrieved from the channel-5 radiance entering the instrument through a spectral filter centered at 6.8 μm . The H₂O product had long standing positive biases relative to other measurements up to this point and therefore it has not been released to the public in the past. Many mechanisms for explaining the biases were evaluated and after much investigation, it was determined that the cause for the biases is the existence of an out-of-band (OOB) spectral leak in the water vapor filter centered at 6.8 μm that is admitting O₃ radiance from the 9.6 μm O₃ band. Prior to now, this radiance was unaccounted for in the radiance forward model used to retrieve H₂O and hence positive H₂O retrieval biases were occurring. More is said about this subject in Section 2 below.

Several contemporary satellite instruments have measured, or are measuring H₂O, spanning different periods over the last two decades or so. These include the Aura Microwave Limb Sounder (MLS) from NASA, JPL (Waters et al., 2006), the ENVISAT Michelson Interferometer for Passive Atmospheric Sounding (MIPAS) from the European Space Agency (ESA) (Fischer et al., 2000), the Scisat-1 Atmospheric Chemistry Experiment-Fourier Transform Spectrometer (ACE-FTS) from the Canadian Space Agency (CSA) (Bernath et al., 2005), and the AIM Solar Occultation for Ice Experiment (SOFIE) from NASA (Russell et al., 2009; Gordley et al., 2009). These instruments have provided H₂O data with prolonged, continuous temporal coverage and with extended spatial coverage. These data sets will be used in this paper to validate the SABER H₂O data.

The logistics of the paper is as follows. In the following section 2 we will present the SABER channel characteristics and briefly introduce the v2.07 H₂O retrieval approach. The SABER error analysis is discussed in section 3. The data sets used for comparisons are described in section 4. In section 5 the global H₂O climatology is examined to serve as an overview and the first glimpse of the SABER H₂O data set. Coincidence profile comparison strategies and results are presented in sections 6–7. The day/night differences in SABER H₂O are evaluated and remaining data issues are discussed in sections 8–9. In section 10 we examine

whether polar mesospheric H₂O seasonal variability is captured faithfully since the most drastic H₂O variability occurs in the polar regions where the eddy driven residual meridional circulation is most active (Dunkerton, 1978; Garcia and Solomon, 1985; Butchart, 2014). Relying on the alternate polar coverage every two months, H₂O variability in the polar stratosphere and mesosphere can be partially revealed. The SABER H₂O long-term time series variability patterns are briefly validated in section 11 via comparisons with MLS and MIPAS H₂O. Conclusions and a summary are given in section 12.

2. SABER channel 5 characteristics and the v2.07 retrieval approach

SABER spectral filter locations and shapes are shown in Fig. 1. The SABER H₂O channel is centered at $\sim 6.8 \mu\text{m}$ as shown by the magenta curve. The forward model used in the SABER retrieval is the BANDPAK model described by Marshall et al., (1994). For individual channels, tables of emissivity growth versus pressure, mass path, and temperature were created for the forward model following the Emissivity Growth approximation (EGA) method described by Gordley and Russell (1981). In the inverse model an onion peeling algorithm (Russell and Drayson, 1972) is applied assuming a spherically symmetric atmosphere. The VMR in the limb tangent layer is adjusted using iterations until the computed and measured radiance values match to within the noise level. This process begins at the highest altitude and proceeds down in altitude always holding the values retrieved at higher altitudes fixed at the VMRs retrieved at those altitudes. We note that in obtaining the current v2.07 H₂O product, the retrieved VMR curve and an a-priori curve based on the Whole Atmosphere Community Climate Model (WACCM), are merged starting at $\sim 83 \text{ km}$ extended upwards. The a-priori and retrieved profile at higher altitudes are combined to obtain a weighted mean value of the two profiles based on the signal-to-noise ratio. This process is needed because at altitudes higher than the mesopause, the SABER channel-5 radiance signal-to-noise level is declining and eventually becomes too low to yield a valid retrieval. The a-priori has only a

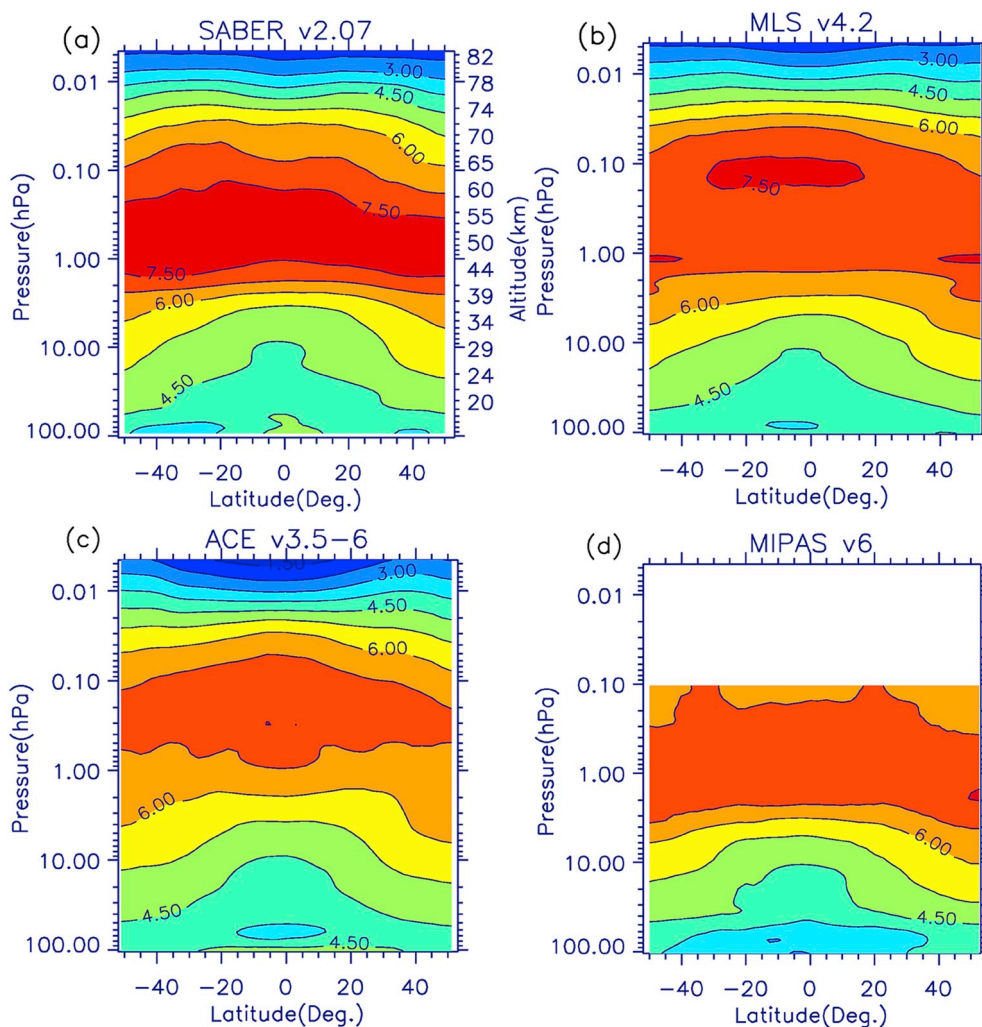


Fig. 4. The pressure (or altitude) versus latitude zonal mean cross-section maps of SABER, MLS, ACE, and MIPAS H₂O averaged over multiple years as long as each dataset is available. For each year the solstice and equinox days are averaged to represent the whole year average. This is to provide a multi-year view of the H₂O distribution with the seasonal cycle removed.

minor effect on the H₂O retrieval below ~83 km and in fact based on the validation results shown later, it is negligible below ~83 km.

SABER H₂O data from prior algorithm versions (i.e., v2.0 and earlier) show consistent positive biases relative to other contemporary data sets and the cause, as shown below, has been determined to be due to out-of-band (OOB) emission leaks coming from nearby atmospheric spectral bands. The problem occurs because the SABER H₂O channel responds to spectral OOB emission primarily due to the 9.6 μm (~1000 cm⁻¹) O₃ band that previously was not included in the retrieval algorithm. Consequently, the additional measured radiance was interpreted in the retrieval process as extra H₂O. The OOB signal comes from atmospheric emission sensed by the instrument in the spectral transmission filter “wings” outside the main in-band filter passband centered at ~1500 cm⁻¹ (the smooth magenta curve in Fig. 1). The blue and purple curves are the simulated radiance for polar winter and polar summer conditions respectively. They exhibit extremely similar shapes. The radiance contributions from the spectral “wings”, i.e. the OOB sources of emission, are dominated by O₃ at 9.6 μm since it is closest to the H₂O channel on the low wavenumber side and has a radiance level much higher than H₂O, i.e., by up to 1–2 orders of magnitude. Note that the H₂O spectral filter transmission is essentially zero at the O₃ emission peaks. However, only a small filter transmission (i.e. ~0.3%) is needed to admit enough radiance to cause a measurable H₂O bias if it is not accounted for in the retrieval. The CO₂ emission centered at ~667 cm⁻¹

is not of much concern because the corresponding H₂O detector response is very small due to its location being far away from the H₂O band center. The OOB problem is a known liability of broad-band infrared limb emission measurements in particular. Such measurements are sensitive to OOB spectral response functions, but they cannot be directly calibrated in the laboratory with sufficient accuracy to ensure adequate modeling of the OOB emission. The correction approach applied to deal with this issue is described below.

The Aura MLS H₂O data set was chosen to determine the SABER OOB radiance corrections because it is widely used and validated. Also it is a high spectral resolution limb emission measurement which, other than SABER, provides the best temporal and spatial coverage available among the current existing H₂O data sets, and it does not depend on non-local thermodynamic equilibrium (NLTE) radiative transfer calculations that complicate the retrieval. The OOB correction approach was to use MLS and SABER data together to determine the additional radiance signal due to O₃ which was then subtracted before the H₂O retrieval process occurred. The correction coefficient was determined using MLS H₂O in the 25–45 km range and SABER O₃ radiances for four one-month periods in 2008 covering different meteorological conditions. In an effort to simplify the fit parameterization we have worked with relative radiance. As a result, both low and high absolute radiance values are nearly equally weighted, thus removing one of the primary reasons we fit to multiple altitude bins, i.e., the absolute radiance values rapidly

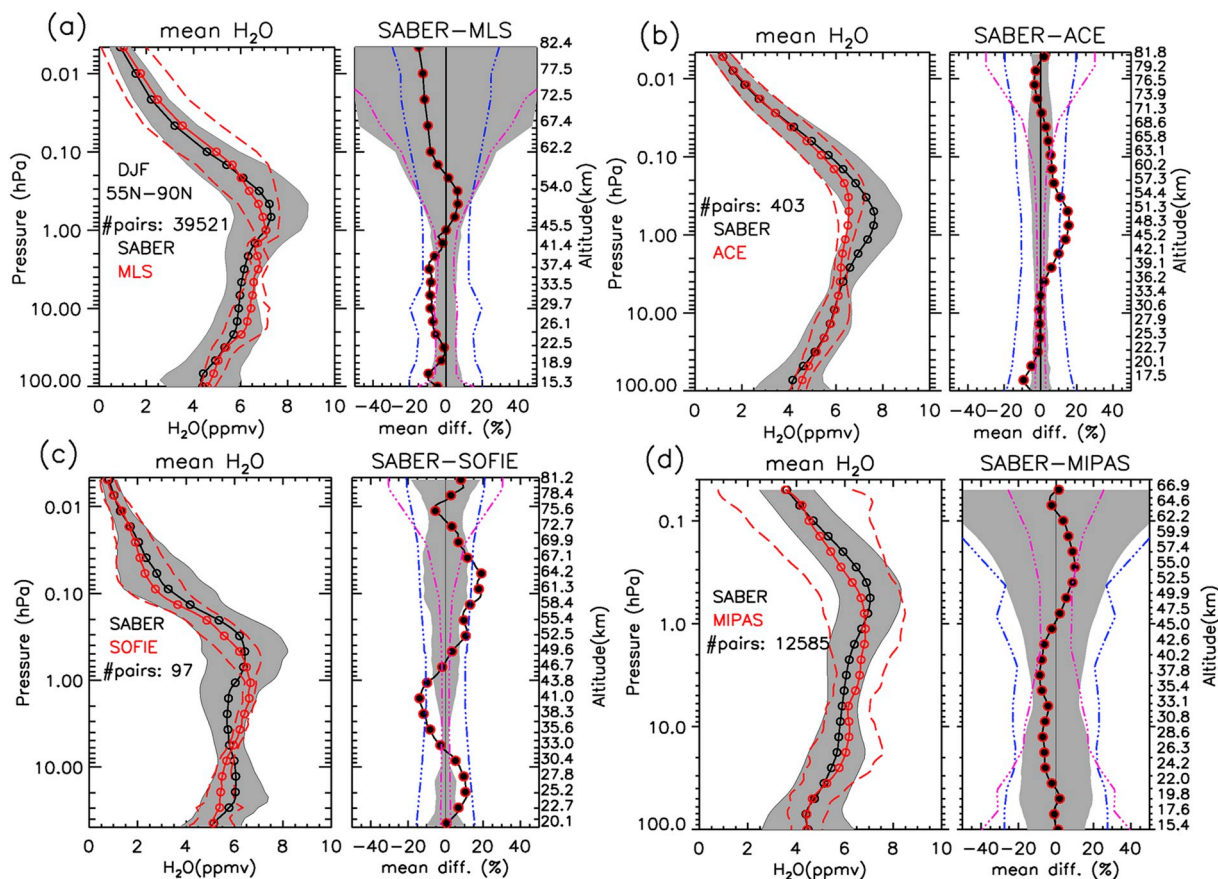


Fig. 5. NH polar winter (55°N-90°N in DJF) profile comparison statistics between SABER H₂O and MLS (a), ACE (b), SOFIE (c), and MIPAS H₂O (d) coincidences, respectively. The left panels are the mean profiles and the corresponding variability ranges (1-σ STD) for the coincidence days in December, January, and February over all the years used. The right panels are the mean differences in percent, with the uncertainty range (gray shade) being the root-sum-square (RSS) of each dataset’s mean single profile precision. The dashed blue and magenta curves are combined systematic and random errors respectively, which serve as the guidance for the mean difference in percent and the combined single profile precision. (For interpretation of the references to color in this figure legend, the reader is referred to the Web version of this article.)

increase as altitude decreases. This greatly simplifies the final fit function and the results suggest that it also achieves more consistent fits over different meteorological conditions. So, we are fitting a relative residual: $(H_2O \text{ Rad}_{(\text{Corrected})} - H_2O \text{ Rad}_{(\text{Measured})}) / H_2O \text{ Rad}_{(\text{Measured})}$, where $H_2O \text{ Rad}_{(\text{Corrected})}$ is the simulated radiance for channel-5. This is fit to measured channel-4 (O_3) radiance relative to measured channel-5 (H_2O) radiance. The result of this process is given in the following equation (1):

$$H_2O \text{ Rad}_{(\text{Corrected})} = H_2O \text{ Rad}_{(\text{Measured})} - 0.00275 \times O_3 \text{ Rad}_{(\text{Measured})} \quad (1)$$

where $H_2O \text{ Rad}_{(\text{Measured})}$ and $O_3 \text{ Rad}_{(\text{Measured})}$ represent the SABER channel-5 (H_2O) and channel-4 (O_3) radiance values and the coefficient 0.00275 has an uncertainty of ~10% over different meteorological conditions. This correction factor was then applied at all other times, altitudes and latitudes for the entire seventeen years of the SABER mission to date. The newly produced H_2O data was screened using a threshold of 12 ppmv in the vertical range of 25 km–80 km to remove a small fraction of the retrievals that give anomalous results as will be detailed in section 9.

3. SABER H₂O error analysis and local time coverage

Table 1 lists the itemized and total systematic and random errors under NLTE conditions at eight altitude levels selected to cover the stratosphere and mesosphere up to just below the mesopause. The SABER error analysis was performed by taking an original “true” unperturbed VMR profile, calculating the corresponding radiance profile using the forward model, and then perturbing the radiance profile by

adding errors. Retrievals were then performed on the perturbed radiance profiles to obtain the updated VMR. When the related error was estimated, all remaining input parameters were set to their nominal values. The resulting error is defined as the 1-σ standard deviation (STD) of a large number of retrievals using the perturbed radiance profiles. The total error is the root sum square (RSS) of errors obtained for each error type.

There are a number of routine systematic error sources in the SABER retrieval. Spectroscopy mainly refers to the uncertainty in the line intensity, assumed to be 1% consistently at all altitudes listed. This will also result in 1% error in the retrieved H_2O VMRs at all altitude levels assessed. The in-band interference from other gases (mainly O_3 and CO_2 and assuming a 10% uncertainty) leads to < 2% errors in the VMR retrieval, and the error decreases toward the higher altitudes as the air density rapidly decreases. The radiance error (~1%) due to imperfect calibration refers to the fact that the background space emission is non-zero. The radiance bias determined in the laboratory is about 1% and results in 2%–5% error response in the H_2O VMRs from the tropopause to 80 km, which is fairly consistent between different channels. It slightly worsens as altitude gets lower since the onion peeling algorithm will cause the accumulation of error. The registration of the SABER radiance profiles with pressure altitude occurs over the range of ~35–45 km. A shift of this region, for example, by ±50 m in this case, leads to 1–3% of H_2O VMR response. Temperature bias is a major error source. The SABER temperature validation study (Remsberg et al., 2008) shows that this bias stays within ±3 K throughout the stratosphere and mesosphere, indicating very good agreement with other data sets in a

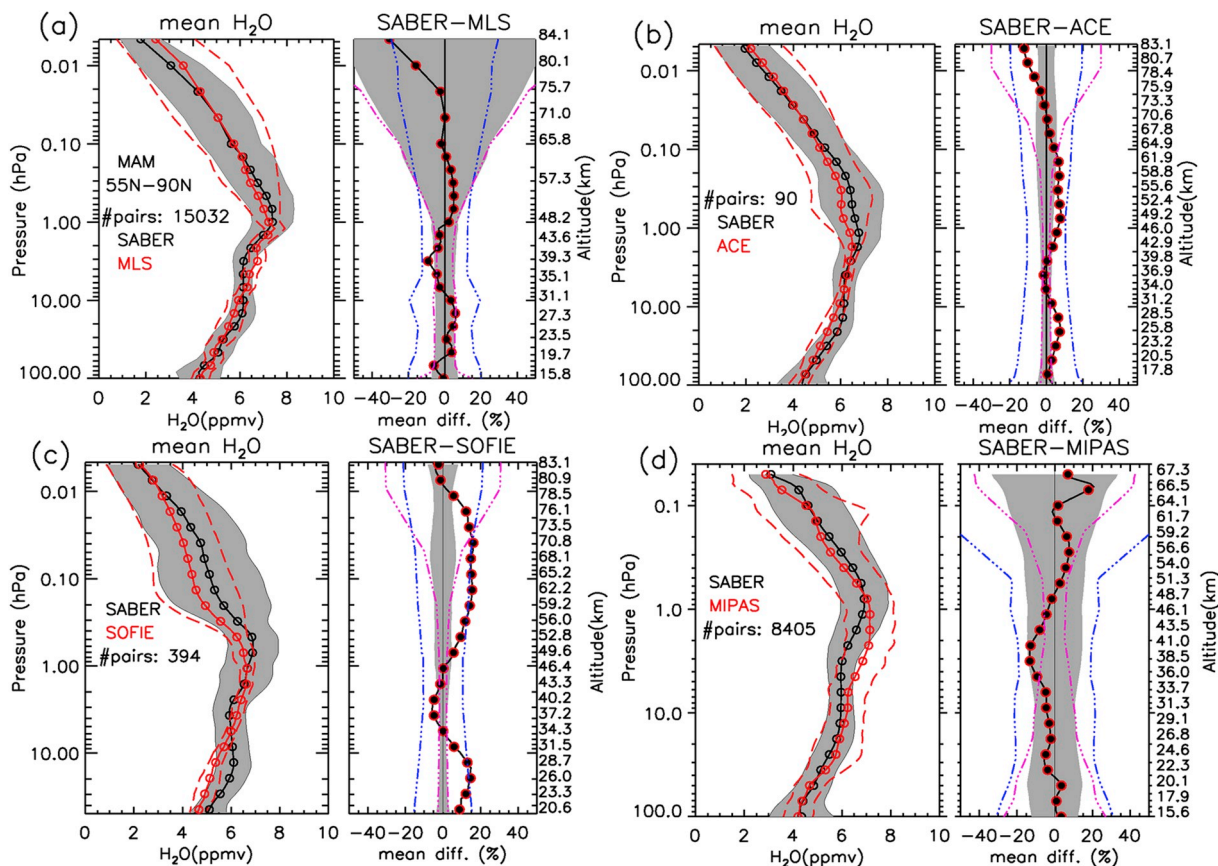


Fig. 6. Same as Fig. 5 except for the NH polar spring in March, April, and May.

general sense. But the H₂O VMR response to the temperature bias is overall the largest among all systematic errors, reaching 20% at the tropopause and remaining as high as 12% up to 80 km altitude. The large response to temperature bias is generally expected in the SABER retrieval because in the infrared spectral range, the radiance is heavily dependent on temperature. This term dominates the total systematic error below 60 km, while above this altitude the error due to the uncertainty of the reaction rates in the NLTE model (Mlynczak et al., 1994; Lopez-Puertas et al., 1995) becomes the largest term. The random error sources include the scan mirror pointing “jitter” (20 m) and the detector noise. The H₂O VMR error response (in percent) to the detector noise rapidly increases above 60 km as the radiance signal becomes weaker in the higher altitudes. The pointing “jitter” causes the VMR response to increase toward the lower altitudes as it is further away along the tangential path. Overall speaking, as shown in Table 1, random errors in SABER H₂O are much smaller below 60 km (~2–4%), suggesting a high precision of the profiles (see profile comparisons in sections 6–7), while above 60 km it rapidly increases to 30%. The total systematic error (10%–20%) increases toward both the lower and upper ends of the altitude range due to temperature and NLTE caused uncertainties respectively. Although the random error close to the mesopause is fairly large we will later show that SABER H₂O displays much better than expected agreement with the MLS and ACE H₂O at these altitudes. Aside from these routine systematic error sources, still there are about ±10% systematic errors unaccounted for based on the validation study shown in sections 6–7.

SABER has unique local time coverage as shown in Fig. 2. The ascending and descending nodes are sampled separately in Fig. 2a and 2b within latitude bins of 5°. For each day the ascending and descending nodes cover two narrow local time ranges that are roughly 12 h apart in the middle to low latitudes. The local time varies only mildly with latitude in the lower latitude region, but the variation becomes more

rapid when it reaches the two ends of the daily latitude range (53°N/S or 83°N/S). What is noteworthy is that SABER local times are different from day-to-day and they slowly shift to cover all 24 h over a yaw cycle (~2 months). This coverage enables a large number of coincidences between SABER and each of the other data sets used.

4. Other data sets used in the study

4.1. Aura MLS

The MLS on the Aura satellite was launched on 15 July 2004 into a 98° inclined 705 km altitude, sun-synchronous circular orbit and is still in operation. The MLS line of sight is in the forward along-track direction of the Aura spacecraft. The Earth’s limb is scanned from the surface to 90 km every 26.6 s giving 240 scans per orbit spaced at 1.5° intervals (165 km) with a total of 3500 vertical profiles per day and nearly global latitude coverage from 82°S to 82°N. MLS measurements are made in five spectral bands, at 118 GHz, 190 GHz, 240 GHz, 640 GHz, and 2.5 THz (Waters et al., 2006). The standard H₂O product (Lambert et al., 2007) used here is retrieved from the 190 GHz (~0.158 cm) band labeled as v4.2 (https://disc.gsfc.nasa.gov/datasets?page=1&keywords=ML2H2O_004). The useful vertical range of v4.2 MLS H₂O is 316–0.002 hPa which is consistent with the earlier versions. The MLS H₂O vertical resolution from 100 hPa to 0.46 hPa (~51±3 km) remains at ~3 km with the systematic error varying in the range of ~5%–19%. At lower pressures the vertical resolution degrades to ~10 km and the systematic error worsens to 23% (at 0.004 hPa or ~83–84 km). Three data quality indices are applied to screen the MLS v4.2 H₂O data, i.e., only profiles with positive precision values, status fields of even numbers, and quality fields greater than 1.45, are valid to use in the science studies. Fig. 3a shows daily repeated MLS local time coverage that takes up two narrow ranges centered at ~02:00 and ~14:00

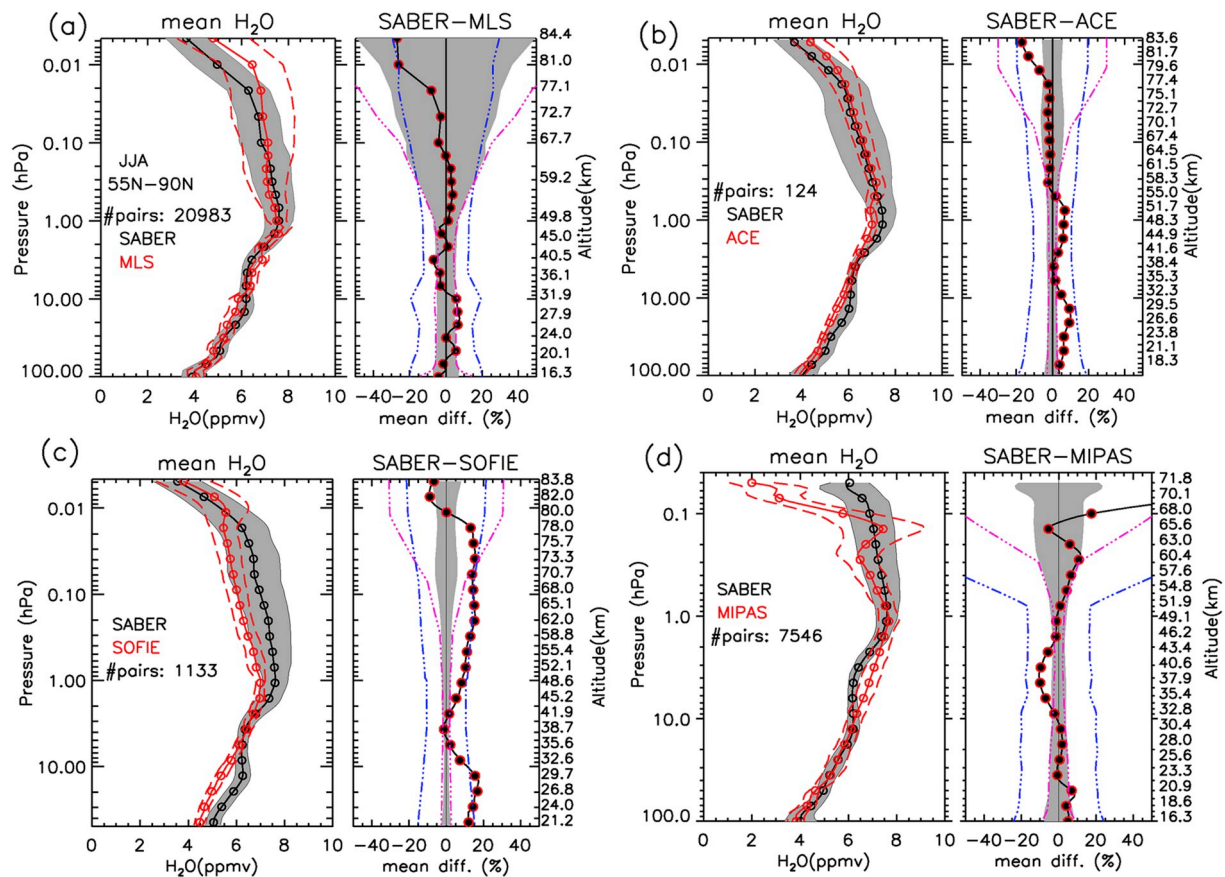


Fig. 7. Same as Fig. 5 except for the NH polar summer in June, July, and August.

respectively in the middle to low latitude range. In the polar region north or south of 50°N/S , a wider range of other local times will occur.

4.2. Envisat MIPAS

The MIPAS instrument on the Envisat satellite (March 2002–April 2012 and 98° inclination sun-synchronous at a mean altitude of ~ 800 km) is a Fourier transform spectrometer for the detection of limb emission spectra in the middle and upper atmosphere using mostly rearward pointing within a 35° viewing angle, obtaining ~ 1500 – 2000 profiles per day. MIPAS observes the infrared spectral range from ~ 4.15 μm to ~ 14.6 μm with a full resolution of ~ 0.035 cm^{-1} originally but a reduced resolution of 0.0625 cm^{-1} since 2005. The MIPAS V6 data set (e.g., Engel et al., 2016; <https://earth.esa.int/web/guest/-/mipas-atmospheric-pressure-temperature-data-constituents-profiles-1547>) used in this study is a reprocessed data set (Raspollini et al., 2006) which covers the complete MIPAS mission including the full resolution phase (July 2002 to March 2004) (e.g., Wetzel et al., 2013), test measurements performed in August to September 2004, and the reduced resolution phase (January 2005 to April 2012). MIPAS is able to detect and resolve a large number of emission features of atmospheric species. The MIPAS products include nitrogen dioxide (NO_2), nitrous oxide (N_2O), CH_4 , nitric acid (HNO_3), O_3 , and H_2O . The MIPAS vertical resolution remains at ~ 2 – 4 km through its valid altitude range < 70 km. The precision, however, rapidly degrades above 50 km. MIPAS equator crossing times are approximately 10am and 10pm repeated every day. The MIPAS local time coverage (Fig. 3b) is sharply residing at these two local times which vary only slightly with latitude. Other local times occur at the extreme polar latitudes which are beyond the SABER latitude ranges suggesting no coincidences between the two data sets under these conditions.

4.3. Scisat-1 ACE

The ACE-FTS on the SCISAT-1 (August 2003 - current and 74° inclination at ~ 650 km altitude) is a high spectral resolution (0.02 cm^{-1}) infrared Fourier transform spectrometer (750 – 4400 cm^{-1} or 13.3 – 2.2 μm) that measures vertical profiles of trace gases and temperature (Bernath et al., 2005). The instrument works in a solar occultation mode with the vertical sampling varying from 1.5 to 6.0 km. The H_2O retrieval uses 54 micro-windows located at central-frequencies of 937.45 cm^{-1} (10.66 μm) and 2992.63 cm^{-1} (3.34 μm). These spectral bands allow profiles to be retrieved from 5 to 101 km altitude [ACE spectroscopy v3.5]. A validation study of ACE measured H_2O was carried out by Carleer et al. (2008) using the earlier v1.0. The v3.5 - 3.6 used in this study is a mixture of versions 3.5 and 3.6 (<https://database.scisat.ca/l2signup.php>). Very small differences are seen between the versions 3.5 and 3.6, with the v3.5 data extending from February 2004 through March 2013 and v3.6 data covering November 2012 onward, with no duplicated periods between the two data versions. The ACE-FTS H_2O single profile precision is given in the data files, which indicates a high precision that remains at $\sim 2\%$ – 4% up to ~ 80 km. ACE has approximately annually repeated local time and latitude coverage with minor shifts as the year increases (see Fig. 3c).

4.4. AIM SOFIE

SOFIE (Gordley et al., 2009) is one of two instruments currently operating aboard the Aeronomy of Ice in the Mesosphere (AIM) satellite (April 2007-current and 97.8° inclination sun-synchronous at ~ 595 – 601 km altitude) dedicated to PMC studies (Russell et al., 2009; Hervig and Gordley, 2010; McClintock et al., 2009). The SOFIE data set provides vertical profiles of temperature, H_2O , CH_4 , O_3 , NO , and CO_2

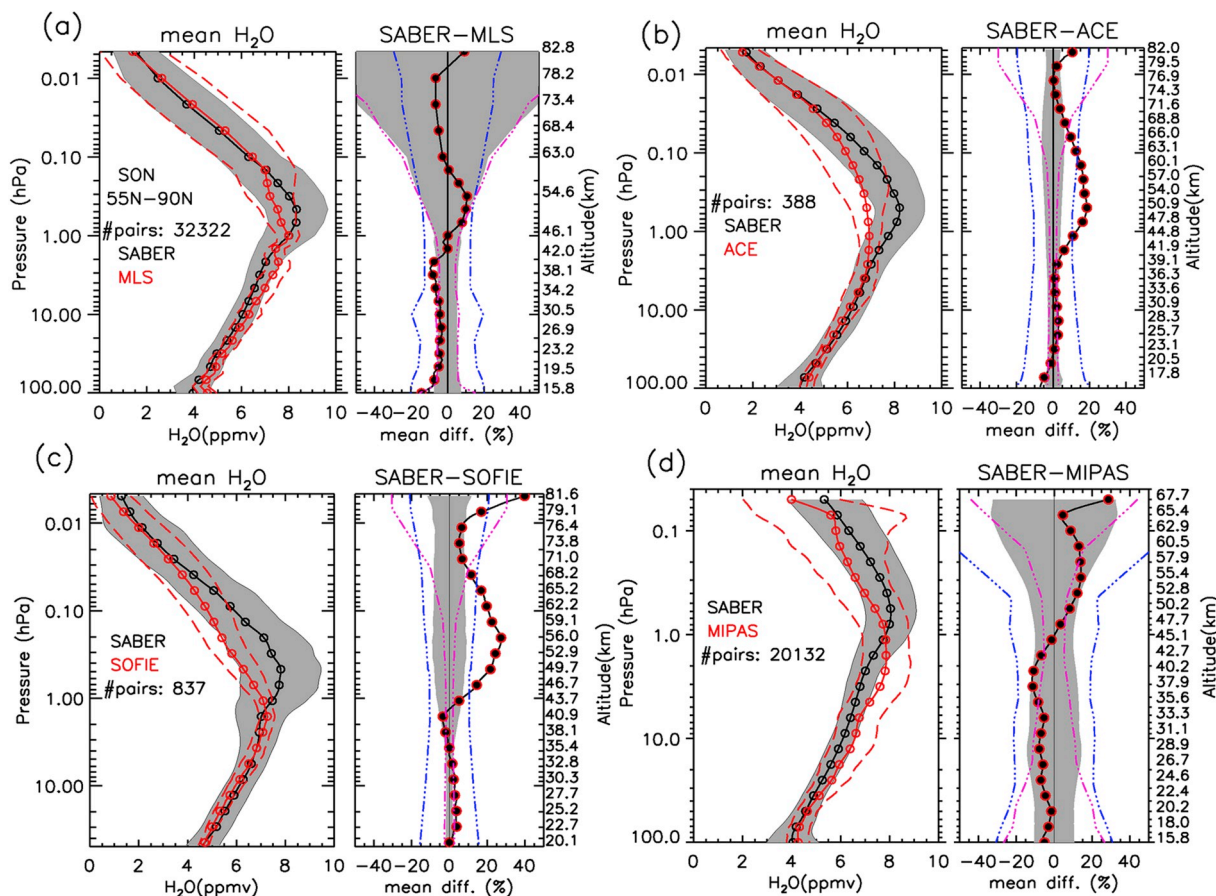


Fig. 8. Same as Fig. 5 except for the NH polar fall in September, October, and November.

which are of great importance in studying chemistry and dynamics in the middle atmosphere. The latest SOFIE data version is v1.3 which is available at <http://sofie.gats-inc.com/sofie/index.php>. AIM is in a polar orbit with a midnight/noon equator crossing time. Therefore its sunrise and sunset measurements occur almost exclusively in the high-latitude regions as shown in Fig. 3d. In 2017 the latitude coverage migrated toward latitudes lower than 50° N/S when the spacecraft approached a full sun condition which existed throughout most of 2018.

Like SABER, SOFIE has a high vertical resolution of 2 km with a consistent vertical measurement spacing of 0.5 km at all altitudes owing to the application of an inter-leave method (Remsberg et al., 2008) in the retrieval to take advantage of all of the measurements. The same approach is applied in the SABER retrieval. The finer vertical spacing can be used to obtain single profile precisions for SABER and SOFIE data sets. Based on the 5-times finer vertical spacing, the single-profile-precisions of both SABER and SOFIE H_2O are obtained by calculating the $1-\sigma$ STD of the values that span the roughly 2 km vertical range (Hervig et al., 2009; Rong et al., 2010) for a given profile. More specifically, the running 2 km window STDs are taken as the precision profile for a given SABER or SOFIE profile. SOFIE H_2O profile precision is generally very high varying from $\sim 0.3\%$ at ~ 45 km to $\sim 5\%$ at ~ 85 km (Rong et al., 2010).

5. Multi-year climatology of H_2O for different data sets

In the analyses that follow, we first examine the SABER H_2O multi-year climatology on pressure versus latitude cross-section grids, shown in Fig. 4a. Aura MLS, Sci-sat1 ACE, and Envisat MIPAS, measured H_2O are shown along with SABER H_2O in Fig. 4b, 4c, and 4d. For each year for a given data set, we used the solstice and equinox days to effectively represent all four seasons. Due to the long chemical life time of H_2O , i.e.,

days to years in the 80 km–20 km altitude range, H_2O does not exhibit persistent day/night differences (Brasseur and Solomon, 2005). We therefore use the combined day/night data to generate the cross-sections. As expected, these figures indicate that in the stratopause and lower mesospheric region (roughly spanning the altitude range of ~ 45 –65 km) a major H_2O maximum exists regardless of latitude. The central altitude however varies moderately with different data sets. It is especially apparent that the ACE H_2O cross-section exhibits a higher altitude peak. Later in the profile comparisons we do find that the H_2O maximum in the stratopause region often occurs at a slightly higher altitude in the ACE profiles than in SABER but the difference mostly stays within 10%. In addition, it is somewhat noteworthy, especially in SABER and MLS H_2O , that there is a mild asymmetry in the mesosphere between the northern and southern hemispheres (NH and SH) with the SH H_2O VMRs being slightly higher. This is probably caused by intrusion of mesospheric low H_2O VMRs during the winter descent (e.g., Randall et al., 2006; Bailey et al., 2014) that causes more intense H_2O reduction in the NH than in the SH (Rong et al., 2016). A similar asymmetry is also observed in the UARS Halogen occultation experiment (HALOE) (Russell et al., 1993) measured H_2O (1992–2005) (Remsberg et al., 2018). The SABER H_2O overall zonal mean climatology agrees better with MLS than with ACE and MIPAS in terms of both spatial distribution and magnitude.

6. Strategies for profile comparisons

The coincidence criterion for SABER and any other satellite data set used for comparisons is 2 h in time, 10° in longitude, and 2° in latitude throughout all the profile comparisons shown in this study. Two hours is a sufficiently strict time coincidence criterion even for constituents with more drastic day/night differences such as O_3 for example.

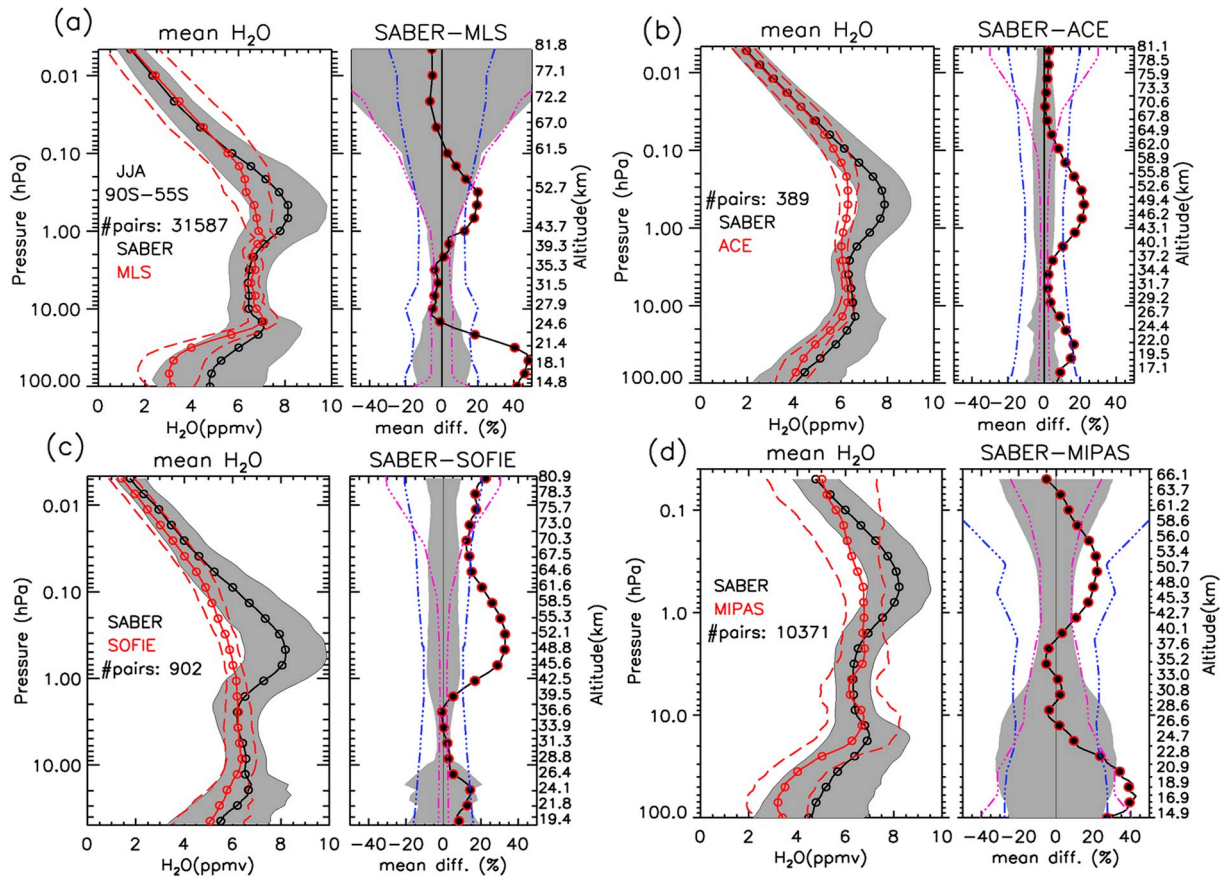


Fig. 9. Same as Fig. 5 except for the SH polar winter in June, July, and August.

Vertical smoothing is applied to the higher resolution data set, i.e., SABER, in all cases for each coincident pair of profiles so that the two data sets are comparable on consistent pressure levels. The least squares fit method is adopted as the main smoothing approach, but as recommended in the MLS data validation and retrieval algorithm studies (e.g., Froidevaux et al., 2008; Livesey et al., 2006) the averaging kernel (AK) smoothing is further applied to the SABER profiles after the least squares fit smoothing when compared with MLS H₂O. The least squares fit method interpolates the higher resolution data set onto the lower resolution data grid using the criterion of minimizing the squared residuals. We should however point out here that different smoothing approaches only cause minor differences in the comparison results and will not affect the conclusions.

The mean difference in percent for all comparisons shown uses the formula

$$\frac{VMR_{SABER} - VMR_{other}}{(VMR_{SABER} + VMR_{other}) * 0.5} * 100 \quad (2)$$

The combined single-profile-precision, defined as the root-sum-square (RSS) of mean single-profile-precisions of each individual data set, is calculated for each pressure level to describe the total random fluctuation in the difference profile of the two data sets being compared. For each data set the mean single-profile-precision is the root-mean-square (RMS) of all the single-profile-precision values for a given pressure level.

The systematic and random errors are obtained from the retrieval analysis, as shown in the SABER error analysis in section 3 and the websites for the other data sets. The combined random error is the RSS of total random errors of the two individual data sets, shown as:

$$error_{com_ran} = \sqrt{error_{ran_SABER}^2 + error_{ran_other}^2} \quad (3)$$

The combined systematic error (e.g., Cortesi et al., 2007) is taken to be:

$$error_{com_sys} = \sqrt{error_{sys_SABER}^2 + error_{sys_other}^2 + SEM^2} \quad (4)$$

where the standard error of the mean differences (SEM=STD/ $\sqrt{\text{number of coincidences}}$) characterizes the statistical uncertainty of the mean difference. The abbreviation STD here refers to the standard deviation of the differences for all pairs of coincident profiles at a given pressure level. Due to the large number of coincidences achieved on a regular basis in the current study, the SEM is virtually zero in most cases. The mean difference in percent is expected to stay within the combined systematic error if the error from the retrieval analysis has effectively included all the primary error sources and the magnitudes of these errors are effectively estimated. Similarly, the combined mean single-profile-precision is expected to be comparable with the combined random error obtained from the retrieval analysis.

To characterize the statistics for different seasons and latitude ranges, we defined seasonal grouping as December, January, and February (DJF), March, April, and May (MAM), June, July, and August (JJA), and September, October, and November (SON), along with the latitude ranges 90°S-55°S, 55°S-25°S, 25°S-25°N, 25°N-55°N, and 55°N-90°N.

7. Results for profile comparisons

7.1. Comparisons in the polar regions (55°N-90°N and 90°S-55°S)

7.1.1. NH polar winter (55°N-90°N in DJF)

The comparisons in the NH polar winter with respect to MLS, ACE, SOFIE, and MIPAS are shown in Fig. 5. The mean profile vertical

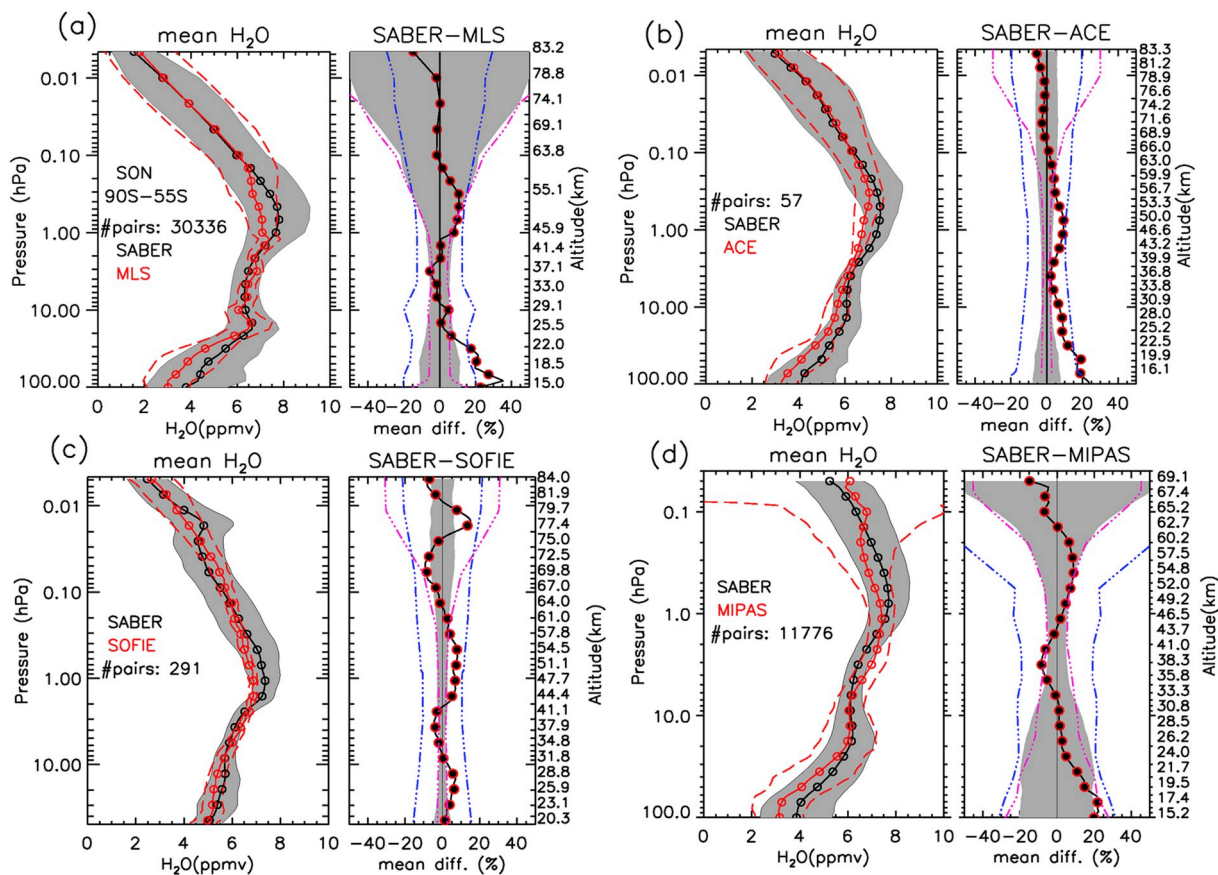


Fig. 10. Same as Fig. 6 except for the SH polar spring in September, October, and November.

distributions are highly consistent between SABER and any of the three data sets suggesting that the balance between the chemistry and dynamics during winter is captured well in SABER. The polar winter H₂O vertical and horizontal distribution mainly results from the dynamical transport driven by the meridional circulation in the mesosphere. The mean differences mostly stay within $\sim \pm 20\%$ on all the pressure levels and with different data sets used for comparisons. In fact in most cases such as with MLS, ACE, and MIPAS the mean differences do not exceed $\pm 10\%$ throughout the stratosphere and mesosphere. With respect to SOFIE, the mean difference reaches 20% in both positive and negative directions. It should be noted that the SOFIE v1.3 H₂O has about 10% negative bias in the mesosphere (Rong et al., 2010) that has served as the main cause for the larger differences from SABER H₂O. But the SABER and SOFIE H₂O mean profile vertical distributions agree well despite the larger biases between the two data sets. Since SOFIE takes measurements in the higher polar latitudes ($>65^\circ\text{N}$), the coincidences encompass the period with significant H₂O depletion associated with the stronger winter or spring descent, leading to a slightly different mean profile shape from the other comparisons shown in Fig. 5.

The vertical distributions of the mean differences are generally consistent among the comparisons relative to the different other data sets used. Except for the ACE comparisons, the mean difference changes sign from negative to positive at $\sim 46\text{--}48\text{ km}$. With respect to ACE, on the other hand, although the vertical distribution is very similar, the entire mean difference profile slightly shifts toward the positive direction so that a positive mean difference persists throughout the vertical range of 35–70 km with the maximum reaching $\sim 18\%$. Above 60 km or below 30 km altitude, it shows less consistent results between different comparisons but it is noteworthy that the agreement is generally close staying within $\sim 5\text{--}10\%$ in the ACE and MIPAS comparisons.

In the SABER versus MLS H₂O comparisons, the combined single

profile precision is close to but slightly exceeds the combined random error, and above $\sim 55\text{ km}$ the difference begins to increase indicating that the combined random error is unable to account for the random variability in the profiles. The mean difference stays within the combined systematic error perfectly throughout the entire vertical range suggesting no unaccounted for systematic bias between SABER and MLS H₂O in this comparison.

With respect to ACE the mean difference exceeds the SABER systematic error in the stratopause region (i.e., $\sim 43\text{--}53\text{ km}$) where the VMR reaches a maximum indicating a significant bias between the two data sets in this range. The combined single profile precision is persistently high ($\sim 2\text{--}5\%$) throughout the stratosphere and mesosphere which suggests that both the SABER and ACE profiles exhibit small random variability. The random variability is far below the level that SABER random error would predict, especially above $\sim 65\text{ km}$ altitude.

The combined single profile precision of SABER versus SOFIE comparisons systematically exceeds the combined random error below 70 km likely reflecting that in the high latitude ($>65^\circ\text{N}$) polar winter, the profiles are more disturbed than in other cases. The combined systematic error also is unable to account for the mean difference in two separate ranges, one in the stratosphere ($\sim 41 \pm 2\text{ km}$) and the other in the mesosphere ($\sim 61 \pm 4\text{ km}$), confirming that the biases between SABER and SOFIE H₂O are significant.

With respect to MIPAS (v6 from ESA) the comparisons are shown only for the altitude range below $\sim 67\text{ km}$ since MIPAS only scans up to 68 km tangent height for the nominal mode measurements. The estimated combined systematic error is almost 3-times larger than the actual SABER versus MIPAS mean difference suggesting a far too conservative error estimate. The combined random error on the other hand is unable to account for the combined single profile precision over an extended vertical range above $\sim 35\text{ km}$. This is mainly caused by the

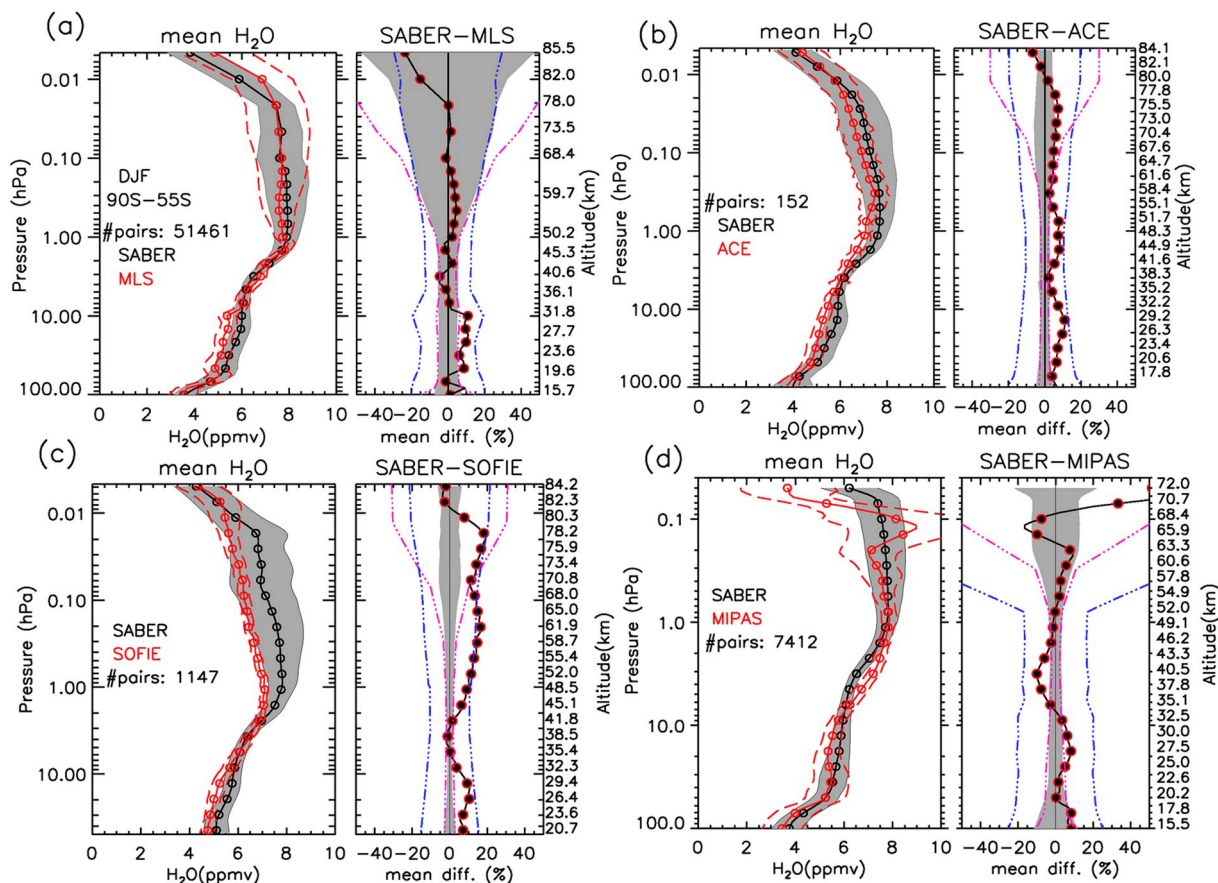


Fig. 11. Same as Fig. 7 except for the SH polar summer in December, January, and February.

large random variability in the MIPAS profiles.

7.1.2. NH polar spring (55°N-90°N in MAM)

The comparisons in the NH polar spring, shown in Fig. 6, also indicate that the mean differences stay within $\pm 10\%$ up to ~ 75 km altitude with respect to MLS and ACE. The agreement in this vertical range is overall slightly better than in the NH polar winter but larger differences did occur in the vertical range of ~ 35 – 40 km where SABER H₂O is biased low by $\sim 15\%$ relative to MIPAS H₂O. The mean profiles in spring consistently indicate higher H₂O VMRs in the mesosphere which reflects a restored H₂O state from the winter low values whereas in the upper stratosphere to stratopause region (~ 35 – 55 km) the VMRs are lower than in winter. These characteristics will also be observed in the following Fig. 23 when the seasonal variability of the polar mesospheric H₂O is examined. The vertical distributions of the mean differences are overall similar to those in winter except that below ~ 30 km altitude, SABER H₂O VMRs tend to be more consistently biased high by ~ 2 – 15% in spring. The mean difference relative to SOFIE again is the largest among all comparisons.

The combined single profile precisions indicate smaller random variability in polar spring than in polar winter in most cases except for the ACE comparisons. The ACE precision is not only generally high but also has the least seasonal dependence. It is also noted that the combined single profile precision and the random error agree exceptionally well below ~ 65 km altitude in MLS, ACE, and SOFIE comparisons. While above this altitude the random error estimate is too conservative in all comparisons shown in Fig. 6.

7.1.3. NH polar summer (55°N-90°N in JJA)

The polar summer represents a very different atmospheric condition from the other seasons due to H₂O enhancement throughout the

mesosphere, especially in the PMC region, caused by the summer polar region upwelling. Fig. 7 presents the NH summer comparisons which indicate that the unique shape of the summer vertical distribution is captured qualitatively well in all the data sets. The agreement between SABER and MLS or ACE H₂O is close below ~ 75 km, with the mean difference varying within $\pm 10\%$. In the range of ~ 50 – 75 km the agreement is even closer diminishing to within $\pm 2\%$ in these two comparisons. The agreement between SABER and MIPAS is close up to the stratopause or slightly above, with the mean difference also staying within $\pm 10\%$. Above ~ 55 km MIPAS H₂O exhibits a noteworthy feature spanning from ~ 2.0 ppmv to ~ 9.0 ppmv that appears to be artificial causing the rapid increase of the mean difference from SABER H₂O. Overall, despite the unique shape of the mean profile in polar summer, the vertical distributions of the mean differences strongly resemble those in the polar spring comparisons. The mean difference with respect to SOFIE is again significantly larger, maintaining a fairly constant percentage of $\sim 20\%$ throughout the ~ 60 – 75 km vertical range.

Above ~ 80 km where PMCs form, the SABER H₂O shows smaller VMR enhancement than in MLS by $\sim 30\%$. Such a negative mean difference is reduced in ACE and SOFIE comparisons, down to ~ 10 – 20% . Due to the fairly coarse vertical resolution in the MLS H₂O in the upper mesosphere (~ 10 km), the enhancement layer produced by the PMC H₂O sublimation could have been more averaged out over a longer vertical range, which is why MLS H₂O usually exhibits a much thicker layer of enhancement (see Fig. 10 of Rong et al., 2010). However, even after the AK smoothing, SABER H₂O is still lower. The differences of SABER and ACE H₂O on the other hand are much smaller and furthermore the vertical slopes of the mean profiles are very similar below ~ 77 km altitude indicating a better qualitative agreement. But since SABER H₂O is biased low with respect to all the data sets used for comparisons it is likely that a real bias in SABER H₂O exists in the PMC

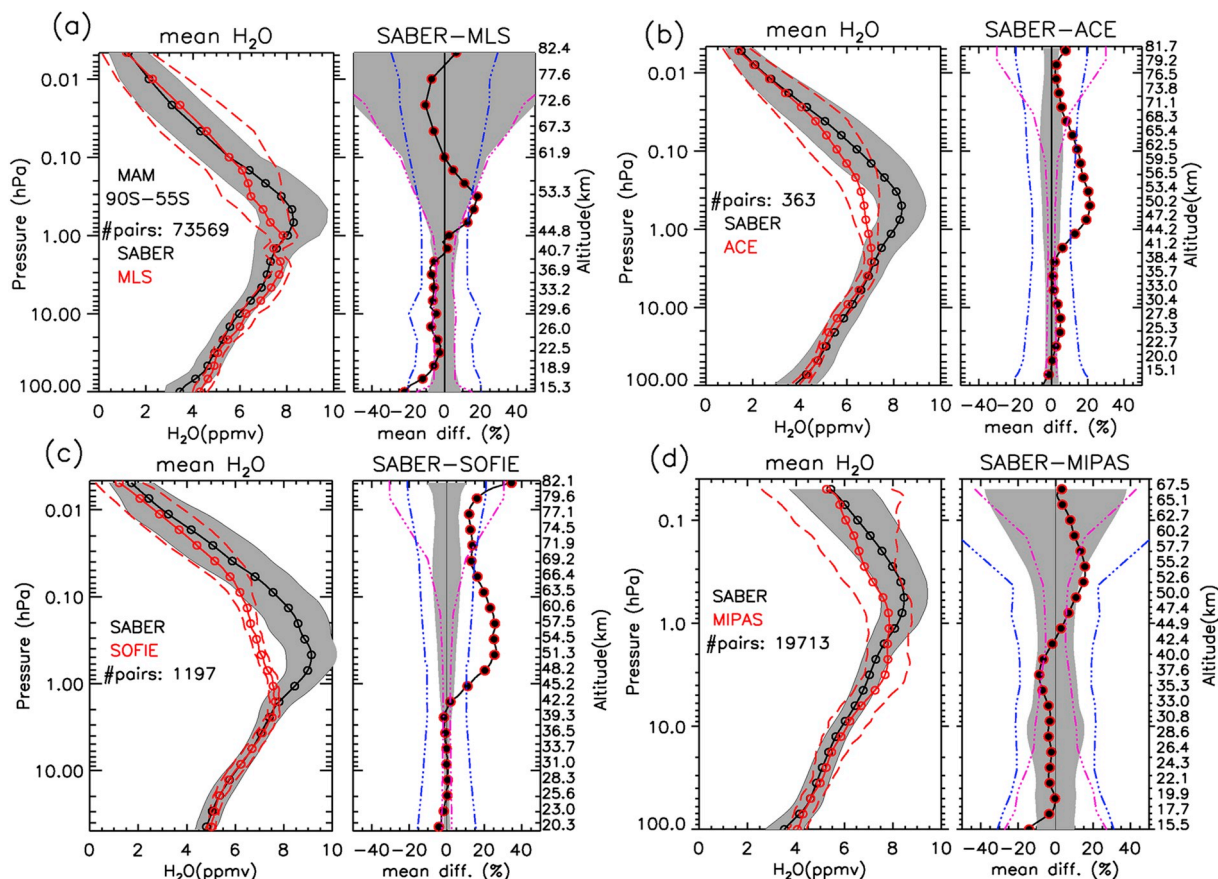


Fig. 12. Same as Fig. 8 except for the SH polar fall in March, April, and May.

region.

The combined single profile precisions are the smallest in summer and nearly precisely agree with the combined random errors below ~60 km in all comparisons while above this altitude the random error estimate is too conservative. These results and those from spring comparisons indicate that the SABER data quality in the middle to upper mesosphere is better than expected. The mean difference stays within the combined systematic error in nearly all cases, and even at the PMC altitudes it only marginally exceeds the systematic error in the comparison with the MLS H₂O.

7.1.4. NH polar fall (55°N-90°N in SON)

When polar summer ends the H₂O VMRs in the mesosphere rapidly decrease to smaller values, as shown in Fig. 8. The mean H₂O profile exhibits an overall similar distribution to those in winter and spring but the H₂O maximum in the stratopause region is consistently stronger in fall. It is shown in Rong et al., (2016) that CH₄ and H₂O are strongly anti-correlated in fall in the stratopause region and the stratopause H₂O peak reaches its annually largest magnitude. Fall is a dynamically quiet season relative to winter and spring (Siskind et al., 2016) and during this time the CH₄ conversion to H₂O might have been the most efficient leading to the annual minimum CH₄ and maximum H₂O in the stratopause region. Although the vertical distributions of the mean differences remain similar to the previous comparisons, the condition of SABER H₂O being higher in the stratopause region relative to the other few data sets is more severe in polar fall than in other seasons.

7.1.5. SH polar winter, spring, summer, and fall (90°S-55°S in JJA, SON, DJF, and MAM)

The SH comparisons share many similarities to their NH counterparts. The SH polar winter (Fig. 9) however is exceptional in the sense

that SABER H₂O is biased high more severely (>20%) in the stratopause region as well as below 25 km altitude. The mean difference exceeds the combined systematic error by a varying percentage from ~5% (MLS) to 20% (SOFIE) in the stratopause region. It should however be remembered that SOFIE H₂O in the SH winter is biased low by ~10% consistently (Rong et al., 2010) which should be accounted for when discussing the difference between SABER and SOFIE H₂O. The comparisons above ~60 km altitude show much closer agreement, especially with respect to MLS (roughly -5%) and ACE (roughly 0-2%). The vertical distribution of the SH winter H₂O mean profile differs substantially from that in the NH winter, i.e., the SH winter profile exhibits a double-peak feature with the upper peak located at the stratopause and the lower peak at ~25 km. SABER H₂O captures both peaks qualitatively well. However the stratopause peak in the SH winter is shown to be broad and weak in the MLS, ACE, and MIPAS H₂O but in SABER H₂O it is stronger (by ~2 ppmv). Rong et al., (2016) (see their Fig. 8) showed that in 2009 when winter descent is significant in both hemispheres, the descent in the SH is weaker but is longer lasting than in the NH and therefore the penetration is down to much lower altitudes (i.e., ~25-40 km). The stratopause H₂O peak was then “fingerprinted” to lower altitudes due to the downward transport. This occurrence lasts through August and September to produce the lower H₂O peak. It appears that larger biases in SABER H₂O often occur close to the H₂O maxima or enhancement features. This should be investigated more closely in future retrieval studies.

In the SH polar spring, shown in Fig. 10, the agreement with all the other data sets used resumed to a much improved state compared to the SH polar winter, i.e., throughout most of the vertical range with the mean differences staying within ±10%. The degree of the agreement between the data sets is similar to the case in the NH polar spring. The agreement above ~60 km altitude is closer than in the NH (varying

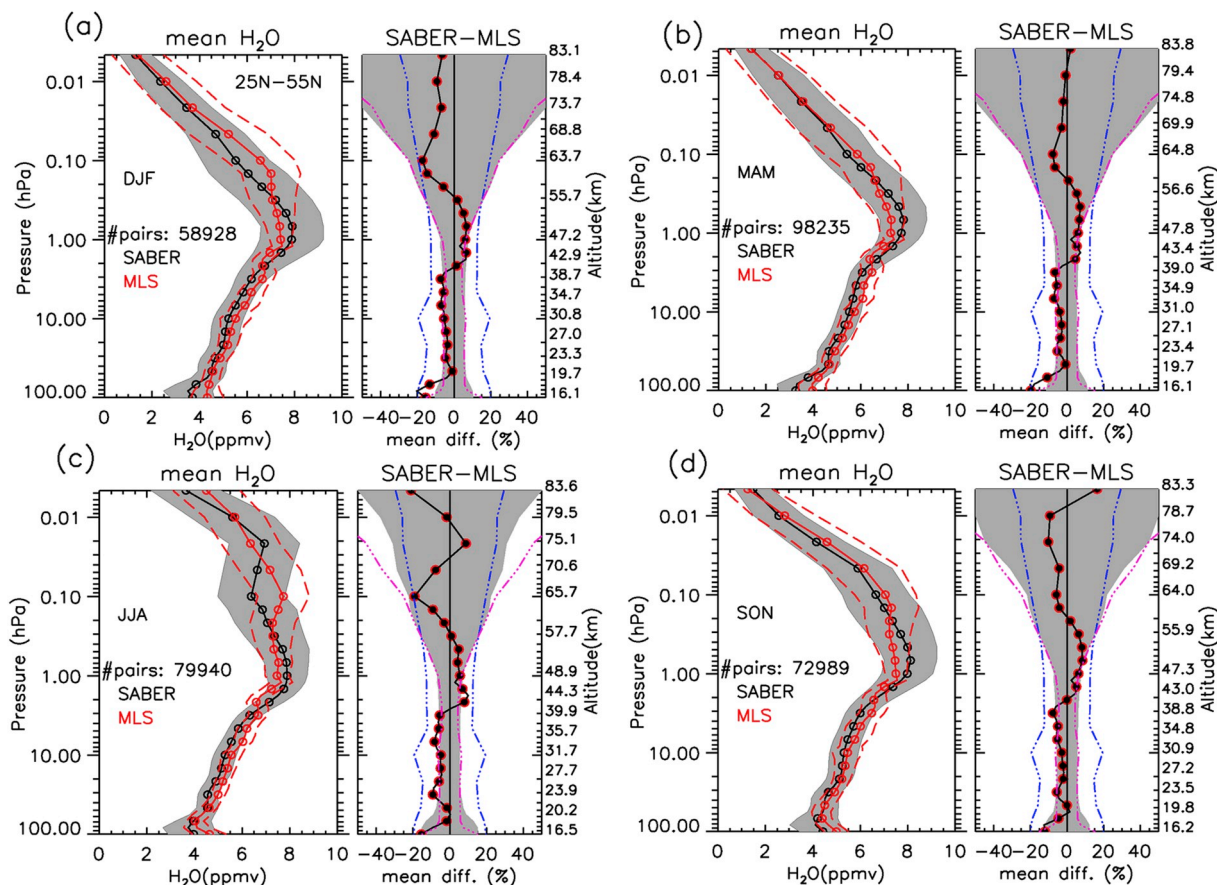


Fig. 13. SABER and MLS NH middle latitude (25°N-55°N) profile comparison statistics for different seasons, (a) DJF, (b) MAM, (c) JJA, and (d) SON.

roughly in the range of -2% to zero below ~ 78 km) with respect to MLS and ACE in particular. In the stratopause region, the SABER H₂O VMRs are biased high by $\sim 10\%$ consistently which is slightly worse than in the NH comparisons. The agreement below ~ 25 km is not as good as in the NH, with the SABER H₂O VMRs being larger by 20% or greater relative to MLS, ACE, and MIPAS. This corresponds to the fact that a hint of the lower peak at ~ 25 km is still present in the SH polar spring. SABER and SOFIE H₂O show better agreement than in the NH throughout the entire vertical range.

The SH polar summer comparisons in Fig. 11 show very similar results to those in the NH polar summer, with the mean differences staying within $\pm 10\%$ with respect to MLS below ~ 78 km, to ACE throughout the entire vertical range, and to MIPAS below ~ 63 km. It is noteworthy that in the SH polar summer the mesospheric H₂O enhancement is overall stronger and furthermore the agreement above ~ 80 km where PMCs exist is $\sim 5\text{--}10\%$ closer than in the NH polar summer with respect to MLS, ACE, and SOFIE.

In the SH polar fall (see Fig. 12) the vertical distribution of the mean differences is also very similar to that in the NH polar fall, although the mean differences in the stratopause region are slightly larger than in the NH by a few percent. In both the NH and SH, the fall season is shown to be the time when the mean differences in the stratopause region are notably larger. Another noteworthy hemispheric difference is that in the SOFIE mean profiles the slope at 65 km in the SH suggests a less rapid H₂O decrease than in the NH. This is likely associated with the condition that SOFIE reaches lower latitudes in the SH MAM than in the NH SON (see Fig. 3d) where mesospheric H₂O reduction is less rapid.

7.2. Middle latitude comparisons (25°N-55°N and 55°S-25°S)

In the middle latitude region (25°N-55°N or 55°S-25°S) the H₂O

VMRs exhibit less strong seasonal variability than in the polar region. For these latitude ranges we present the four seasons together to closely examine their seasonal variability.

7.2.1. Comparisons with MLS in the 25°N-55°N range

The SABER versus MLS comparisons in the range of 25°N-55°N are shown in Fig. 13. For each season the shapes of the mean profiles agree qualitatively well between the two data sets. In winter the slope in the mesosphere indicates much less H₂O depletion than in polar winter, and accordingly in this case the winter and spring H₂O mesospheric vertical distributions are drawn closer. Further on in fall there is an upward “bulged” shape indicating a less rapid “post-summer” H₂O VMR reduction than in the NH polar fall (in Fig. 8). In summer the vertical distribution suggests enhancement in the mesosphere in both SABER and MLS but SABER exhibits a mild double-peak feature that is mainly caused by the profiles toward the higher latitude limit at $\sim 52^\circ\text{N}$. This would cause SABER H₂O to be biased low by $\sim 20\%$ which is marginally contained in the combined systematic error. Otherwise the overall vertical distribution and magnitude ($\pm 10\%$) of the mean differences between the two data sets is very similar to other comparisons with MLS H₂O shown above.

7.2.2. Comparisons with ACE in the 25°N-55°N range

The comparisons with ACE in the 25°N-55°N range (in Fig. 14) share many similarities to the MLS results (in Fig. 13) which include, i.e., the winter and spring profile slopes drawn closer than in the polar region; more elevated mesospheric H₂O VMRs in fall in this latitude range than in the polar region; and a hint of a SABER double-peak in the summer mesosphere although is less distinct. A notable small scale fluctuation of the mean profiles is present because fewer coincidences are achieved (see Fig. 3c).

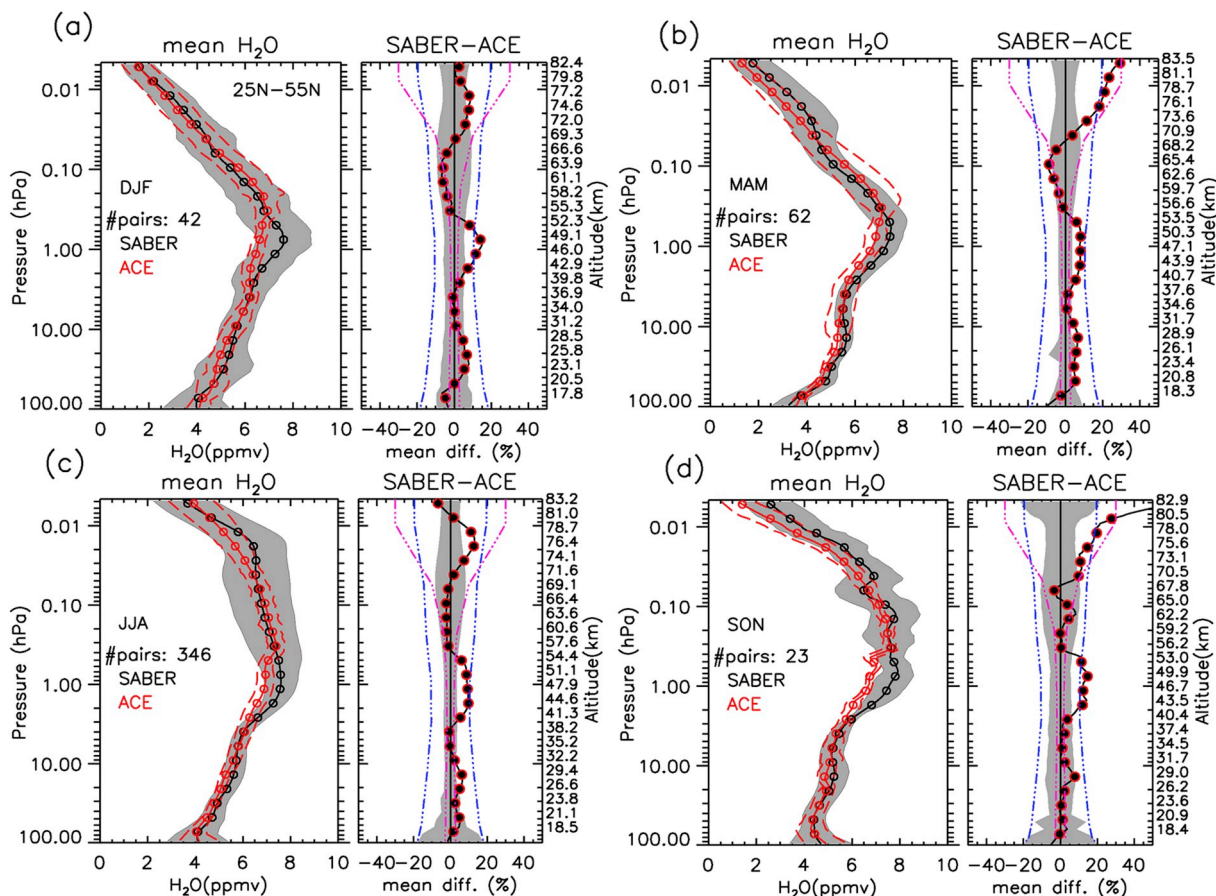


Fig. 14. Same as Fig. 13 except for the comparisons between SABER and ACE.

The mean differences shown in Fig. 14 mostly stay within $\sim 10\text{--}15\%$ indicating overall very good agreement between SABER and ACE in the NH middle to high latitude range. Like in the other comparisons with ACE shown above, the mean differences of SABER and ACE H₂O VMRs suggest that SABER H₂O VMRs are more consistently biased high. In addition, in spring and fall in the upper mesosphere (>70 km), SABER H₂O is biased high systematically reaching 20% or greater at ~ 83 km altitude, which is not echoed in the comparisons with the MLS H₂O. This is attributed to the different sub-sets of the profiles that the two comparisons cover.

7.2.3. Comparisons with MLS and ACE in the 55°S-25°S range

The comparisons with MLS in the SH middle latitude range (55°S-25°S) (in Fig. 15) show very similar results to those in the NH except for a few minor hemispheric differences. First, in both the SH winter (JJA) and SH fall (MAM) comparisons, the agreement is notably closer (i.e., by 5–10%) than in the NH counterparts above ~ 60 km altitude. Second, the mean profiles suggest that in the SH winter and spring the mesospheric H₂O VMRs appear slightly larger. This probably echoes the minor asymmetry shown in the zonal mean H₂O climatology (see Fig. 4).

The same comparisons with ACE (in Fig. 16) also indicate similar results to those in the NH. In addition, similar to the MLS comparisons (shown in Fig. 15a and b), the SH winter and spring H₂O VMRs in the mesosphere (in Fig. 16a and b) also exhibit more upward “bulged” shape indicating larger VMRs than in the NH.

7.3. Low latitude comparisons (25°S-25°N)

The climatology shown in Fig. 4 indicates that in the equatorial region the H₂O VMR vertical peak region is broadened toward the mesosphere and meanwhile appears to be “pushed” upward slightly in the

stratosphere. These characteristics will be echoed in the profile comparisons throughout Figs. 17–19 as shown below.

The SABER versus MLS comparisons in the 25°S-25°N latitude range are shown in Fig. 17. The mean differences stay within $\pm 10\%$ in most cases occasionally exceeding 15% and are within the combined systematic error at all times. The vertical distribution of the mean difference is tremendously consistent between different seasons and also resembles most of the previous comparisons between SABER and MLS H₂O. In the equatorial region the seasonal variability is almost absent but there is a notable semi-annual variability reflected by larger VMRs in DJF and JJA in the upper mesosphere close to 80 km altitude.

The same comparisons with ACE H₂O (in Fig. 18) also show almost no seasonal variability and a highly similar broad and slightly lifted vertical peak region. In the stratopause region SABER H₂O is biased high from ACE H₂O by 10% consistently which is a known condition. Another noteworthy feature is that the mean profile shapes in the mesosphere are remarkably similar between SABER and ACE although the actual VMR values are increasingly separated toward the higher altitudes. As a result, the mean differences stay within 10% up to 75 km altitude and then increase to $>20\%$ at 83 km in all panels shown.

The comparisons with MIPAS are also shown for the low latitude range (see Fig. 19). The vertical distribution of the mean differences resembles the previous MIPAS results, characterized by a consistent negative-to-positive conversion at ~ 43 km altitude in this particular case. It is worth noting that the combined single profile precision tracks the combined random error closely in the altitude range of 25–60 km. The MIPAS systematic error again is far too conservative to serve as any guidance about the mean difference. The MIPAS comparisons in the mid-latitude region were not shown to avoid redundancy, because they tend to show highly similar results to those in the current figure.

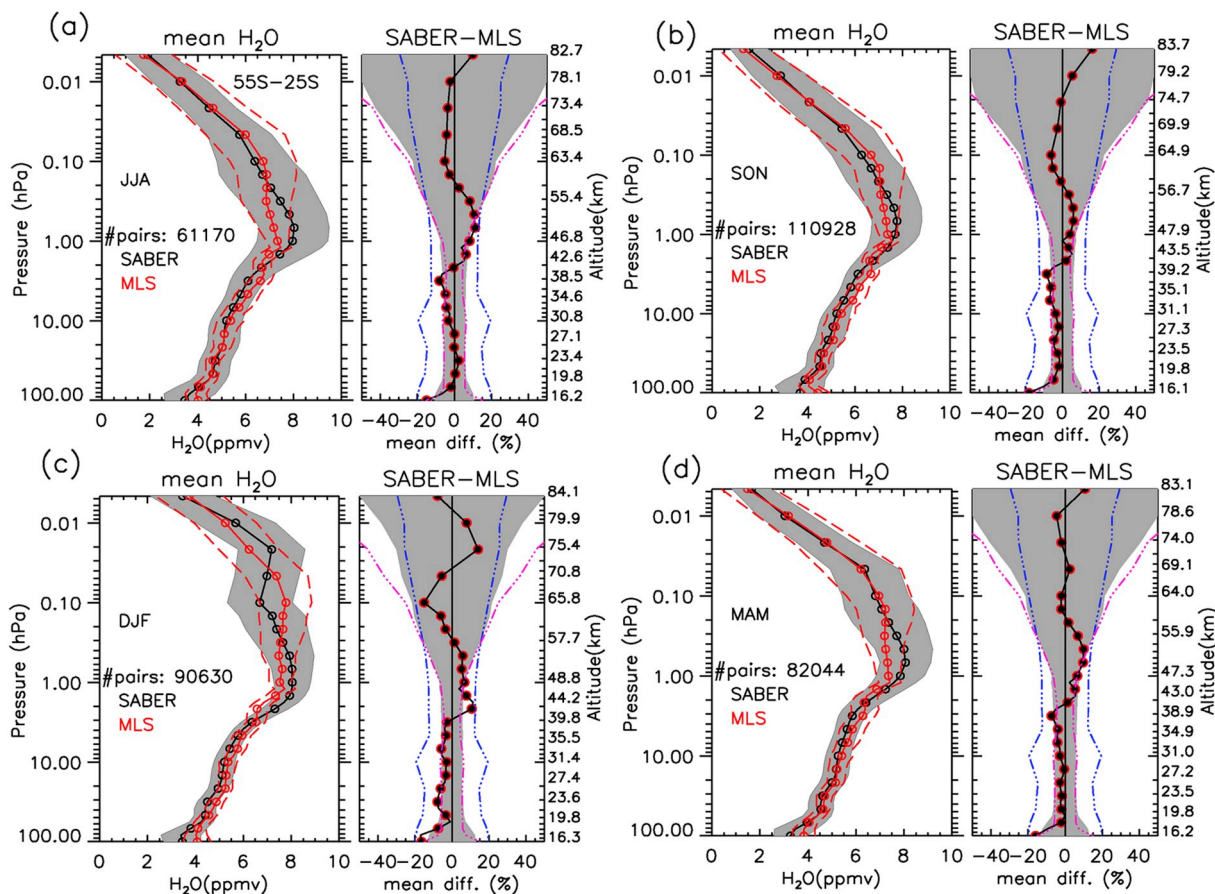


Fig. 15. The comparisons between SABER and MLS (as in Fig. 13) except for the SH middle latitude range 55°S-25°S.

8. Day/night differences

The diurnal variability in mesospheric H₂O can reach notable magnitudes in the upper mesosphere even though extensive studies on this topic are still lacking to our best knowledge. Understanding and characterizing SABER H₂O day/night differences is important in its own right because of the challenges faced in the H₂O NLTE retrieval caused by radiative transfer complexities and reaction rate uncertainties.

Day/night coincidences are analyzed separately for the NH polar spring and summer (55°N-90°N) using the 2005 and 2010 data combined to obtain the statistics (see Fig. 20). The results show distinct day/night differences in both SABER and MLS H₂O. Furthermore, in either day or night, the mean profile vertical distributions agree very well and the mean differences stay within 10–15% in most cases. The daytime mean profile (in Fig. 20a) appears to be characterized by higher mesospheric H₂O VMRs that exceed the nighttime values by 1–2 ppmv, which is shown more clearly in Fig. 20e. The downward intrusion of the low H₂O in the winter to spring time appears to be more distinct on the night side of the measurements. The fact that SABER and MLS H₂O both show similar day/night differences in the polar spring makes it more credible but future studies are required to examine the mechanisms. The results in polar winter and fall, although not presented, are very similar to those in the polar spring in terms of the day/night differences. The analysis to the H₂O observation at ALOMAR in northern Norway (69°N, 16°E) by Hallgren and Hartogh (2012) confirms the existence of diurnal tidal variability (but with a smaller magnitude of ~0.3–0.4 ppmv) in the vertical range of ~65–80 km. This is presumably caused by the tidal wind transport mechanism because H₂O production (destruction) is excluded due to the long chemical lifetime of H₂O on the order of days to weeks.

The polar summer H₂O, on the other hand, is known to possess a

unique vertical distribution and therefore should be examined separately. The NH polar summer day and night H₂O (in Fig. 20c and 20d) show intriguing yet enlightening results. Revisiting Fig. 7c we find that the mixture of both day and night coincidences show very similar profile shapes to the daytime only results in Fig. 20c. This is expected since the polar summer coincidences are dominated by the daytime measurements, i.e., 3296 in daytime versus 218 at night in this particular comparison. Yet the smaller number of nighttime coincidences exhibit noteworthy profile shapes. Above ~75 km altitude, SABER and MLS nighttime profiles both exhibit a double-peak feature and possess more strongly enhanced H₂O than the daytime profiles (see Fig. 20f). Although the double-peak feature shown in the SABER nighttime profiles may very well reflect a realistic feature, the overall lower VMRs (i.e., by ~25%) in SABER at PMC altitudes could indicate a real low bias relative to MLS in the NH summer, which has also been shown in the profile comparisons. Overall speaking, if ascent is the sole mechanism of the H₂O enhancement in the polar summer, then the nighttime transport appears to be slightly stronger.

In the equatorial region (25°S-25°N in MAM) coincidences with MLS H₂O were also found and compared for day and night respectively, as shown in Fig. 21. Fig. 21c indicates that the SABER H₂O day/night differences remain at ~2 ppmv in the mesosphere, while for MLS H₂O the day and night vertical distributions are almost identical showing essentially no differences. The daytime SABER H₂O vertical distribution agrees qualitatively well with the daytime MLS H₂O while the nighttime SABER H₂O shows apparently lower H₂O in the mesosphere and higher H₂O in the stratopause region. Such a profile shape of SABER H₂O is, however, not found in the coincidences with ACE or MIPAS (in Figs. 18 and 19), which indicates that only some fraction of (equatorial) profiles exhibit this shape. In summary, the nighttime vertical distribution of SABER H₂O in the equatorial region has some important differences

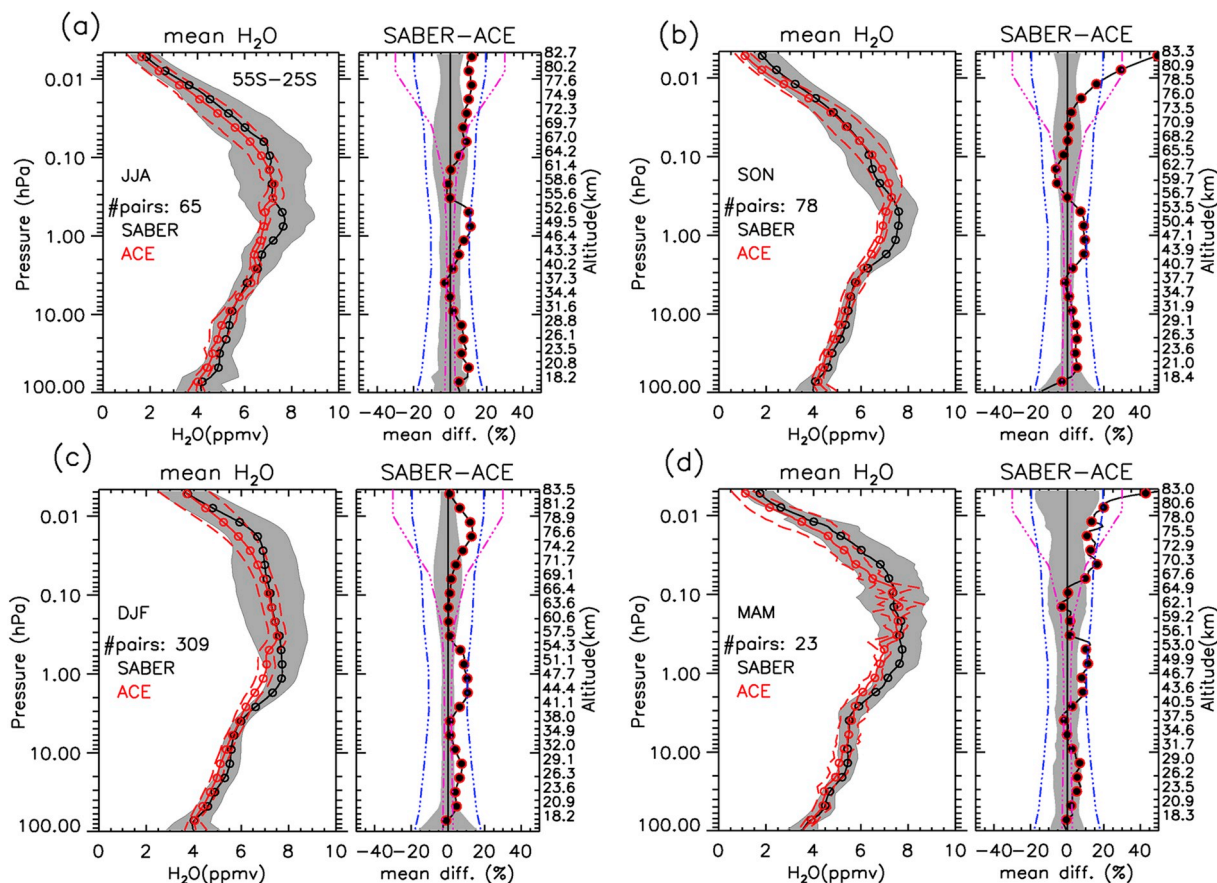


Fig. 16. Same as Fig. 15 except for the comparisons between SABER and ACE for the SH middle latitude range 55°S-25°S.

relative to MLS H₂O. The magnitudes of the differences however do not exceed the variability ranges (red dashed line and gray shade) which indicates that they are not statistically significant but should be investigated further for any causing mechanisms.

9. Discussion of other data features

After examining all the profile comparisons shown above, we next address the question of whether the larger differences relative to the other data sets coincide temporally and spatially with the times and latitudes at which larger fractions of rejected profiles occur. Note that the data validation shown above is only for the useful profiles after the screening criterion (given in section 2) was applied. The SABER H₂O retrieval has been challenging because the limb emission measurements in the infrared spectral range are strongly affected by NLTE processes. The OOB correction, along with the constrained upper boundary and the NLTE model, has been effective in curbing these problems to produce a significantly improved product. Yet in some cases the percentage of the rejected profiles can reach 20% which is fairly high. To provide a more detailed evaluation, we present the fraction of useful profiles identified over the course of a year in Fig. 22a which indicates that in spring and fall the fraction of useful profiles reaches up to ~98% whereas in winter and summer it can fall below 80%. July especially, is the month when the largest number of rejected profiles occurs, and we further sampled these profiles within the 5° latitude bins, as shown in Fig. 22b. Results show that the majority of rejected profiles occurred in the SH high latitude region. The profile comparisons above have echoed this by showing that in the SH polar winters, the mean difference is the largest. Further, it is noteworthy that at 50°N/S, especially in the SH, there are spikes indicating anomalously higher number of rejected profiles compared to other latitude bins. Other than being the starting or ending

latitudes to the alternate yaw cycles these latitudes do not seem to hold any special meaning. These spikes of rejected profiles at 50°N/S are curious occurrences and should be investigated further. It is worth pointing out that in many cases these large values coincide with the summer mesospheric high latitude region where large temperature gradient occurs (not shown). The limb viewing geometry assumes spherically symmetric layers of atmospheric property and therefore when a strong horizontal gradient occurs, the retrieval accuracy will be affected. But this effect has not yet been evaluated quantitatively. In addition, the known low bias at the PMC height in the polar summer region is not echoed by any notably larger fraction of rejected profiles in this region. The equatorial region is also not a region where a high percentage of rejected profiles occurred even though it is where day/night H₂O difference does not closely agree with MLS.

10. Polar winter and summer H₂O pressure versus time cross sections

Primarily driven by the mesospheric residual circulation (e.g., Dunkerton, 1978; Garcia, 1989), polar mesospheric H₂O exhibits stronger variability than in the lower latitude region. Although SABER only achieves partial time coverage north/south of 53°N/S due to the yaw effect, it is important to validate the SABER H₂O variability in this region in a qualitative sense. The zonal mean H₂O over the course of a year is shown in Figs. 23–24 for SABER, SOFIE, and MLS for the years 2009 and 2011. The winter and spring descent and the summer enhancement are the two noteworthy features to be closely examined. The data are sampled at the SOFIE NH latitude ±1° for a given day. These two years were chosen to demonstrate the cases with strong and weak meridional transport (e.g., Siskind et al., 2016). In 2009 strong descent began in late January and persisted through February and

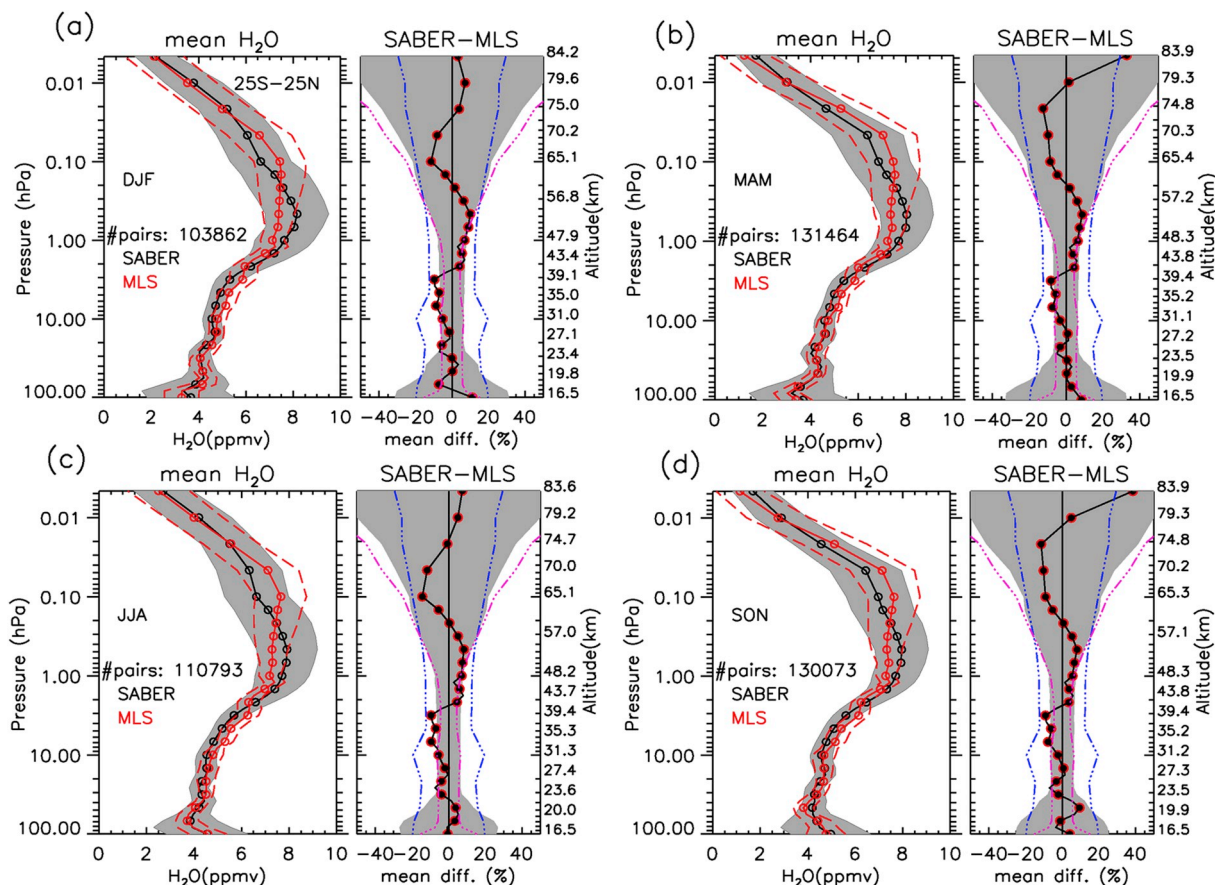


Fig. 17. The comparisons between SABER and MLS for the equatorial latitude range (25°S-25°N).

March until mid-April. In May the H₂O VMRs began to restore throughout the stratosphere and mesosphere due to both upward transport in the mesosphere and the enhanced H₂O due to CH₄ chemical conversion in the stratosphere. The latter produces the stratopause H₂O peak region that reaches the smallest and largest magnitudes in late spring and fall respectively (Rong et al., 2016). The winter and spring descent is captured extremely well in SABER H₂O. Although SABER H₂O also captures the summer mesospheric enhancement and the strengthening stratopause H₂O maximum in fall, a few differences are worth noting between SABER H₂O and the other two data sets. Overall, SABER and MLS H₂O agree better in magnitude and both are higher than SOFIE H₂O, which is expected due to the SOFIE low bias mentioned above. However, SABER H₂O exhibits somewhat different isopleth slopes than the other two data sets during the summer months when measurements are available. Starting from October the slope of the rapidly decreased H₂O VMRs and the isopleth gradient are well captured in SABER but the stratopause peak appears to be too strong (by ~0.8–1.6 ppmv based on the color bar) which is also seen in the profile comparisons. The H₂O variability in the winter and spring of 2011 is drastically different from that in 2009 in the sense that there is no descent feature at all. This inter-annual variability in polar winter and spring is captured well in SABER H₂O. The polar summer in 2011 also has the same problem as in 2009 regarding the isopleth slopes, suggesting that it is a persistent issue throughout the years. In summary, throughout most times of the year, especially during winter and spring, SABER H₂O faithfully captures the characteristic variability patterns. But the polar summer data quality probably requires further evaluation through the actual usage of SABER H₂O in future PMC studies.

11. Long-term variability

11.1. SABER 2002–2017 time series compared with MLS and MIPAS

Although obtaining the H₂O response to the 11-year solar cycle or extracting the long-term linear trend is not in the scope of this paper we will next briefly compare the long-term time series from different data sets. Extracting the long-term variability from any retrieved property is generally challenging because the shorter term variabilities are much stronger and any associated uncertainty may affect the determination of these variability modes. In addition, data sampling or instrument status may induce biases that can accumulate over time. But with all these potential challenges, the retrieved SABER H₂O response to the 11-year solar cycle is very reasonable as shown below. Fig. 25 shows the global mean (50°S-50°N) daily long-term time series over the years 2002–2017 on a series of pressure levels for SABER, MLS, and MIPAS H₂O. Due to the different vertical resolutions of the data sets, we may observe aliasing of the vertical fluctuation into the time series. A universal 60-day smoothing is applied to the daily time series to reduce such effects. In addition, to only compare the variability patterns between data sets, we subtract the respective multi-year average from the series.

The SABER and MLS long-term time series agree exceptionally well on all pressure levels selected throughout the stratosphere and mesosphere. At the upper altitude limit of 0.00464 hPa (roughly at 84 km) both data sets show strong semi-annual variability patterns with amplitudes of 1.0 ppmv to 2.0 ppmv. In the SABER H₂O retrieval at this altitude, the WACCM a-priori values are heavily weighted and yet both the semi-annual variability and the hint of the 11-year solar cycle agree well with MLS H₂O. The 11-year solar cycle response implies a high H₂O at solar minimum in 2009 (Hervig and Siskind, 2006). On the 0.046 hPa pressure level (~69 km), the mixture of annual and semi-annual cycles

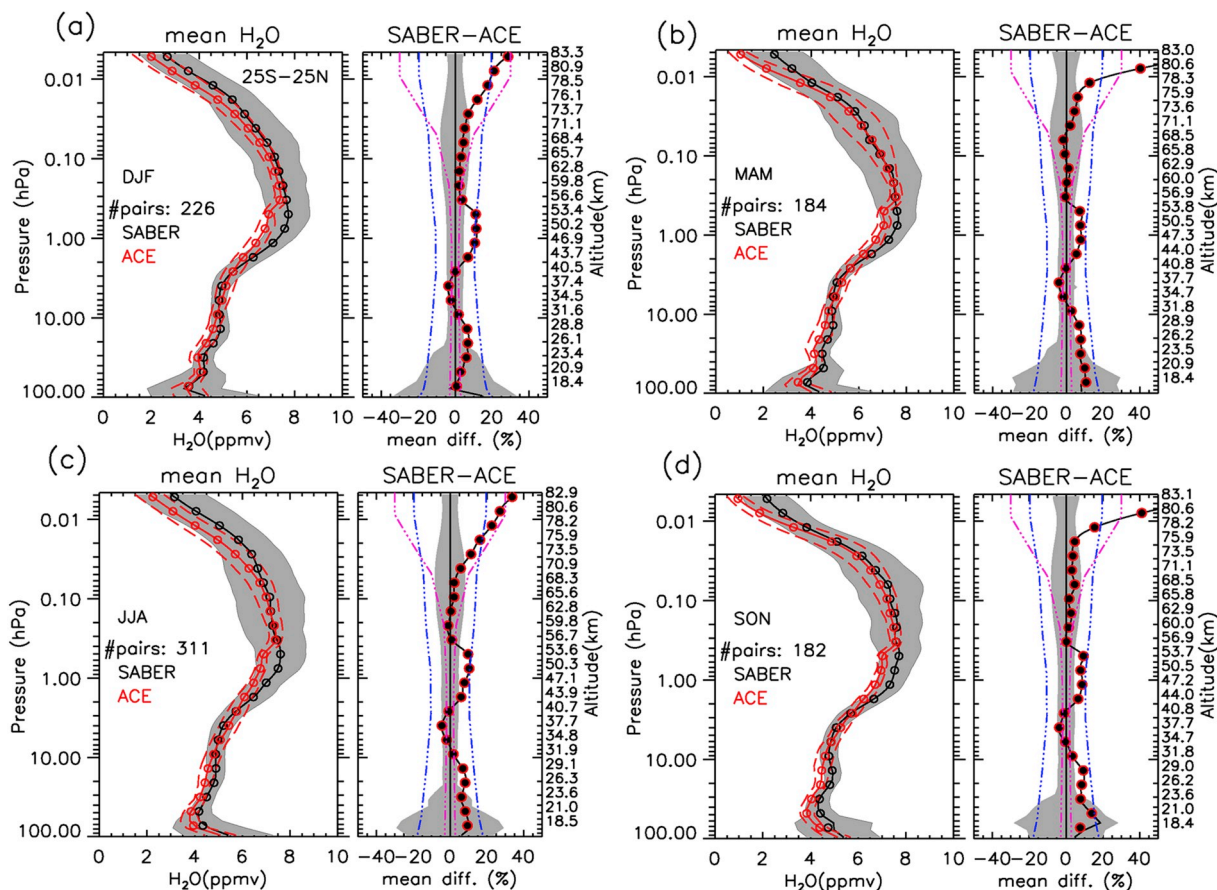


Fig. 18. Same as Fig. 17 except for the comparisons between SABER and ACE for the equatorial latitude range (25°S-25°N).

makes the variability pattern less organized yet the agreement with MLS remains quite close and the response to the 11-year solar cycle is also in the same direction. On the pressure levels 0.22 hPa (~59 km) to 2.6 hPa (~40 km) the variability patterns are similar, mainly exhibiting a multi-year variability with an approximately four-year period and an amplitude of ~0.6 ppmv overlapped with a smaller amplitude (~0.2–0.3 ppmv) of mixed annual to semi-annual variability. The solar cycle response is not visually recognizable on these pressure levels. On the pressure levels 8.3 hPa (~32 km) and 14.7 hPa (~28 km), more of an irregular variability pattern appears, exhibiting a prolonged trough roughly centered at around 2007 and a narrower peak in 2013. It looks like a solar cycle response of a reversed sign compared to the upper mesosphere. At 82.5 hPa (~17 km) the solar cycle response is also not clear but the annual cycle becomes dominantly strong reaching amplitudes of ~1.5 ppmv. Overall, it appears that the solar cycle response is only distinct and visually detectable in the upper mesosphere while at the lower altitude levels, it is much less distinct. In addition, on most pressure levels, there appears to be a somewhat upward linear trend over the last 17 years.

The annual to semi-annual variabilities in MIPAS data also agree quite well with SABER and MLS, but MIPAS H₂O exhibits more significant decadal scale variability at altitude levels of 40.6 km and 32.4 km, resembling a solar cycle response that is not clearly recognizable in the SABER or MLS H₂O time series at the same altitude levels. The MIPAS H₂O series is not shown at 51 km or higher altitudes because the deviation becomes increasingly larger. Yet the comparisons with MIPAS serve as a key validation due to its data availability prior to 2005. Comparisons are made between SABER and MIPAS time series in smaller latitude bins and it is found that the agreement can be close in certain latitude ranges such as in the equatorial region which is shown in Fig. 26. Larger deviations from the SABER or MLS time series shown in

Fig. 25 are likely caused by the higher latitude MIPAS data.

11.2. Tropical tropopause H₂O “tape-recorder”

The SABER H₂O data set was further assessed to determine its ability to reveal the tropical tropopause tape recorder phenomenon (e.g., Mote et al., 1996). This term has been used to describe the hypothesis that air passing through the tropopause is marked in a way that resembles a magnetic tape being stamped by the recording head (Mote et al., 1996). In this case, the tropopause annual cycle modulates H₂O as it enters the stratospheric “over-world” in the tropics as shown in Fig. 27a. The fluctuation amplitude is attenuated at higher altitudes, i.e., from ~2–3 ppmv to <1 ppmv, and it takes about 18 months for the signal to propagate from 100 hPa to about 20 hPa. The variability patterns overall look very similar between SABER and MLS H₂O as shown in Fig. 27. For example, both data sets show qualitatively the same inter-annual and longer time scale variability throughout the vertical range. It is especially worth noting that the stratospheric H₂O increased with time over the last decade in both data sets. However, in the lowest part of the altitude range (i.e., 80–100 hPa), SABER H₂O is ~0.6 ppmv smaller than MLS H₂O and SABER H₂O features are more vertical in this altitude range suggesting a more rapid ascent. In the higher altitude range (i.e., <50 hPa) the ascent rates appear to be quite similar between the two data sets. It is worth pointing out that below an altitude of ~22 km, about 58 ± 3% of SABER H₂O profiles include values that exceed a 12 ppmv rejection threshold above the tropopause (not shown). This occurs because of the fact that when the center of the SABER Field-Of-View (FOV) scans the earth limb, the FOV wings view into the upper troposphere on the low altitude portion of the scan. This causes the radiance signals to be contaminated by cloud emission that is falsely interpreted in the retrievals as large lower stratosphere VMRs (>>100 ppmv). The

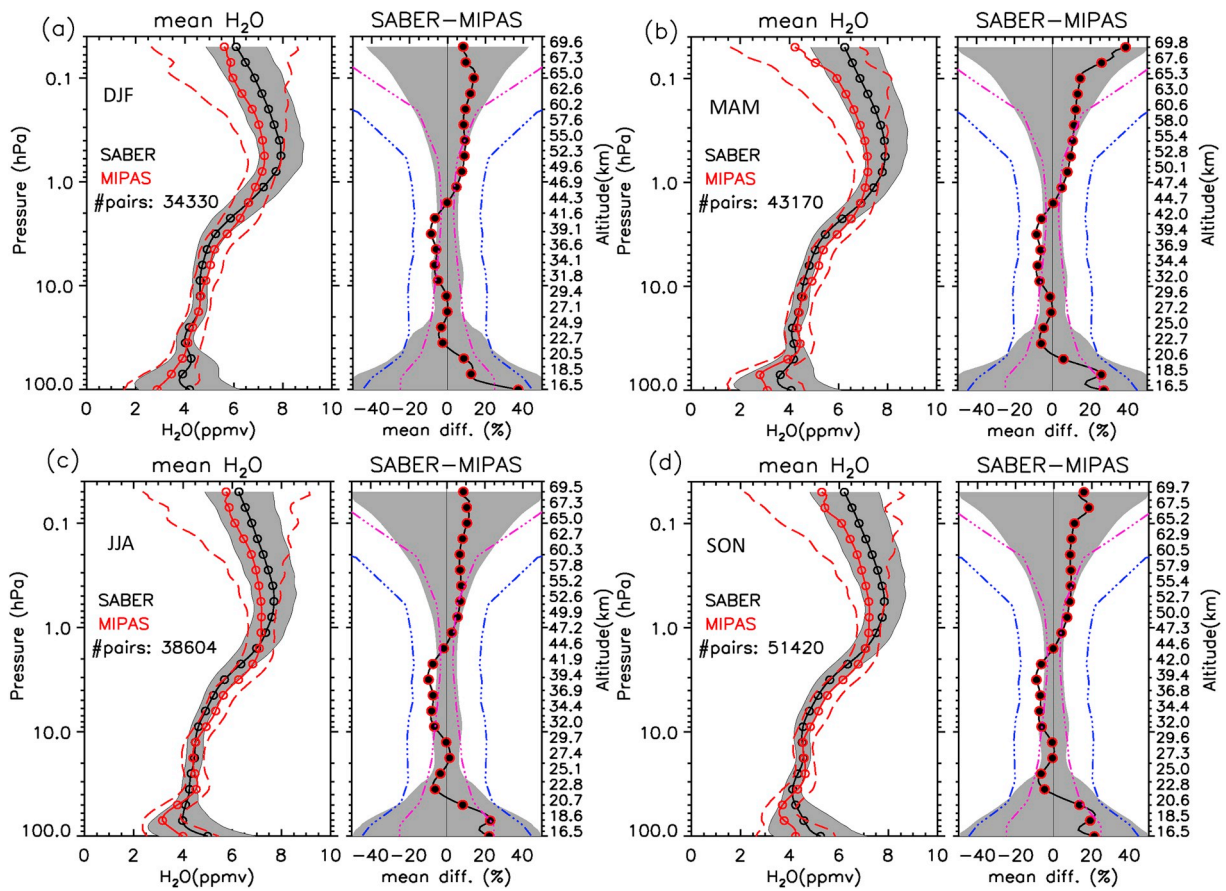


Fig. 19. Same as Fig. 17 except for the comparisons between SABER and MIPAS for the equatorial latitude range (25°S-25°N).

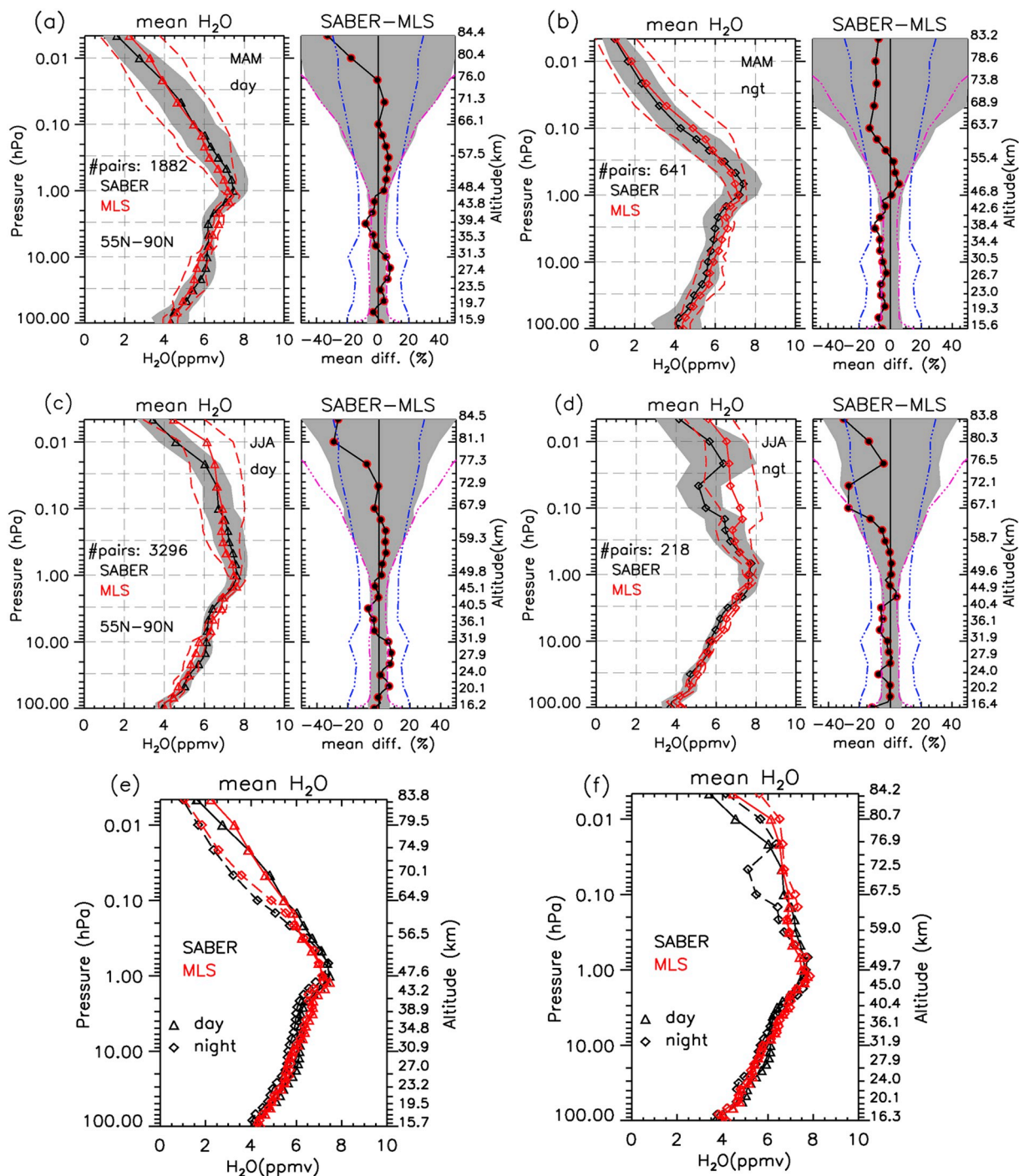


Fig. 20. SABER and MLS coincident profiles comparison statistics for day (a) and night (b) in polar spring (MAM) using the combined 2005 and 2010 data. (c-d) are the same except for polar summer. In addition, in (e-f) the day and night mean profiles are plotted together for polar spring and summer respectively after regrouping the curves in Fig. 20a and b.

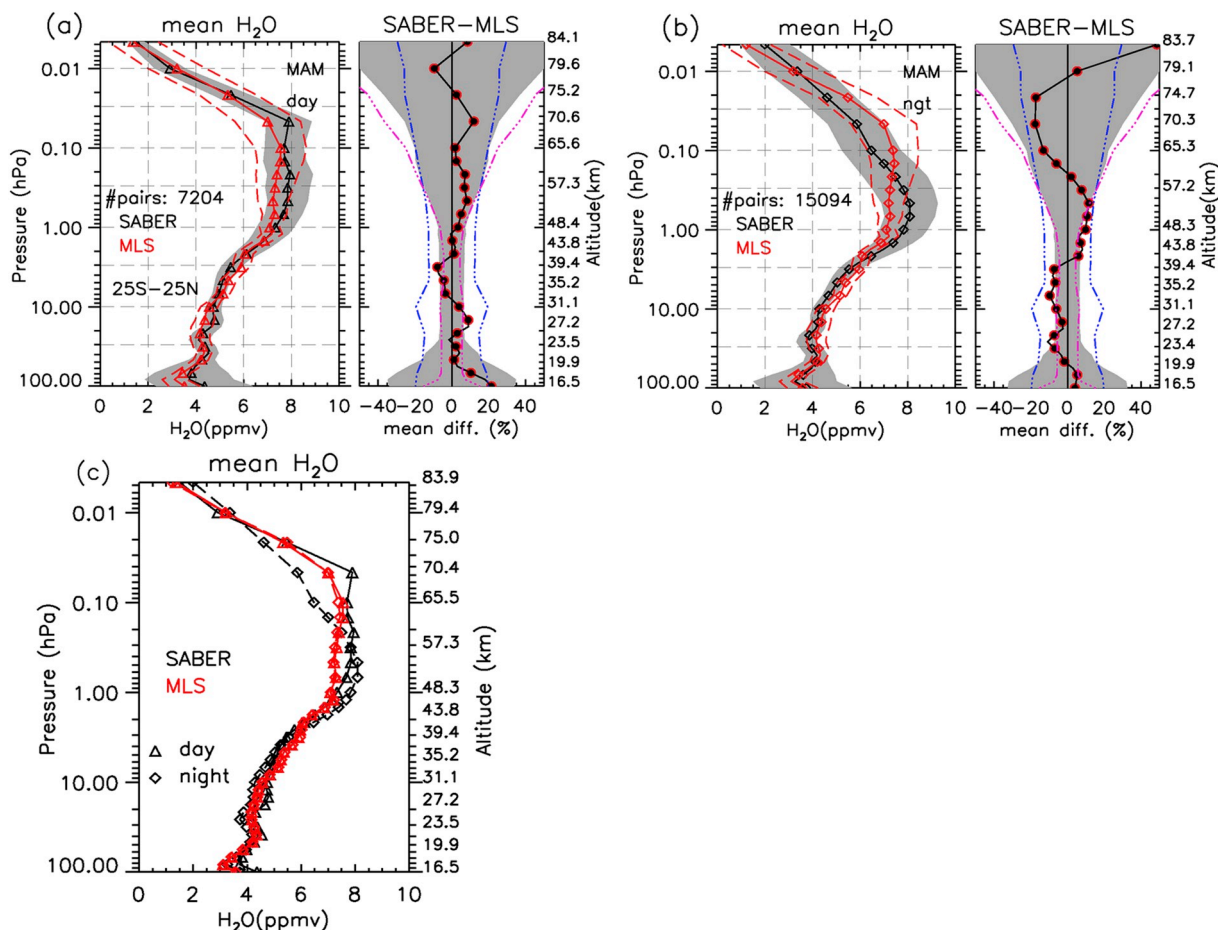


Fig. 21. Similar to Fig. 20 except for the analysis for the equatorial region. In this case the MLS H₂O day and night vertical distributions are nearly identical whereas SABER H₂O still exhibits significant day/night differences in the mesosphere.

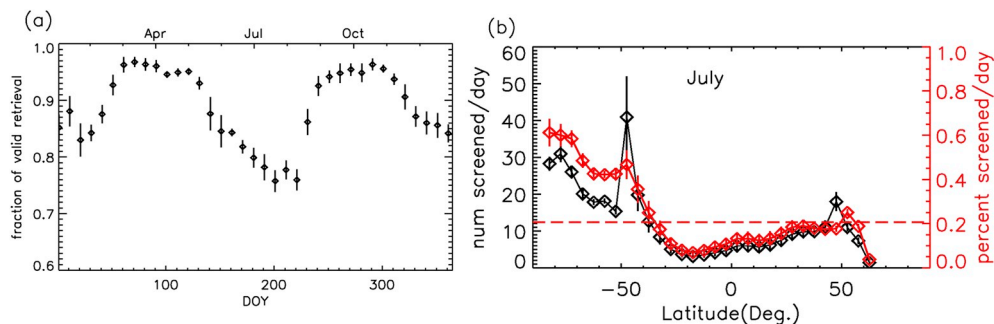


Fig. 22. (a) The fraction of valid SABER v2.07 H₂O profiles over the course of a year. The uncertainty range is the standard error of the mean (SEM) over years 2003, 2008, 2013, and 2017. (b) Since July has the poorest percentage of the valid profiles, it is investigated further over 5° latitude bins. In each bin the mean daily number of invalid profiles averaged over all days of July, and the corresponding percentage, are shown by diamond signs. The uncertainty range is the SEM of the four years chosen. The dashed horizontal line is the mean percentage over all latitudes.

remaining $42 \pm 3\%$ of the SABER scans lead to useful retrievals in the tropics down to ~ 100 hPa, and these are the profiles used to produce the “tape recorder” shown in Fig. 27.

12. Conclusions and summary

An out-of-band (OOB) correction approach is applied to the SABER channel 5 (centered at $\sim 6.8 \mu\text{m}$) radiance to retrieve the v2.07 H₂O VMRs throughout the stratosphere and mesosphere. The OOB emission comes from the spectral “wings” outside the main in-band spectral response function. The OOB leak is a known liability of broad-band infrared limb emission measurements. In the infrared spectral range,

the channel that is observing a lower radiance in the band center will be more strongly impacted by higher radiance levels emitted from nearby emission bands. For example, the O₃ emission bands are closest in spectral location to the H₂O band and they emit a radiance level 1–2 orders higher than that from H₂O. A sub-set of Aura MLS H₂O measurements, selected throughout the year 2008, was chosen to make comparisons between coincident SABER and MLS H₂O profiles in order to derive a radiance correction coefficient that represented the effect of OOB emission due to O₃ on the H₂O channel radiance so it could be removed before retrieval.

The SABER H₂O random error from the retrieval analysis stays within 4% below 60 km altitude while above this it rapidly increases to

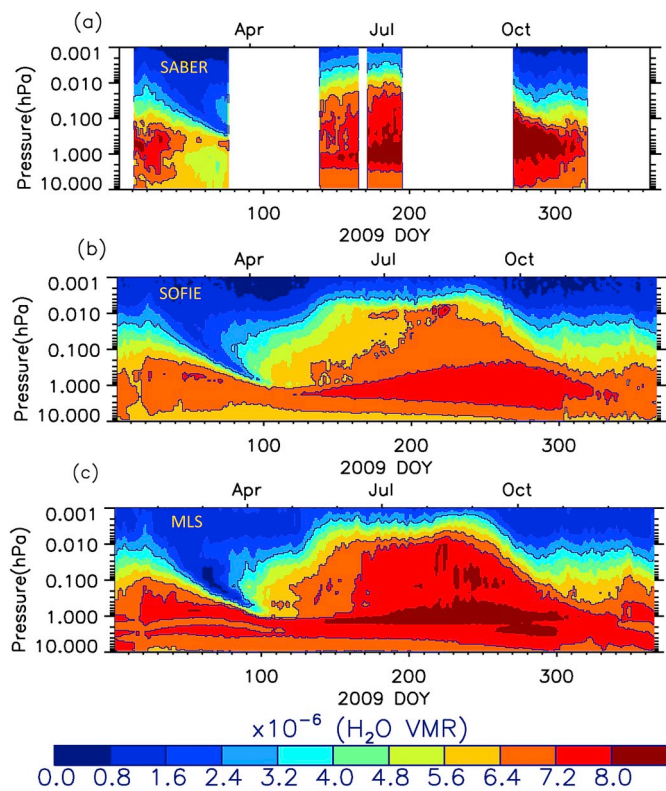


Fig. 23. The 2009 NH polar region pressure versus time cross-sections of H₂O at the SOFIE latitudes ±1° using SABER (a), SOFIE (b) and MLS (c). The year 2009 is chosen because strong descent occurred in this winter.

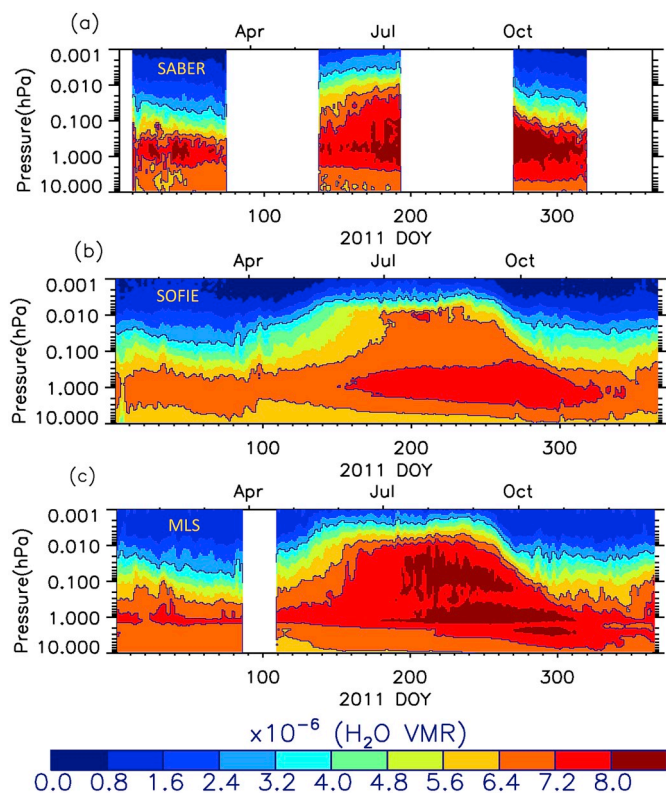


Fig. 24. Same as Fig. 23 except for the year 2011. This year is chosen because it has a notably weak winter descent which is opposite to the case in 2009.

~30% mainly due to measurement noise. The noise increases rapidly above 80 km altitude and accordingly the signal-to-noise becomes increasingly low. The valid vertical range therefore does not go higher than the PMC height (~83 km) for the SABER v2.07 H₂O product. The systematic error is dominated by the temperature uncertainty caused errors that vary between 10% and 20% from 15 km to 80 km. Above 60 km systematic errors caused by the NLTE model become significant, reaching 15% at 80 km. The error response in the NLTE model primarily stems from the uncertainty in the reaction rates. The total systematic error of the SABER v2.07 H₂O is about ~10–20%.

The profile comparisons shown in this paper include a large number of combinations of latitude ranges and seasons, along with different other data sets used, but they share many similarities with some noteworthy differences in some seasons or latitude ranges.

The SABER H₂O mean profile vertical distributions in the stratosphere and mesosphere agree qualitatively well with all the other data sets used in all seasons and latitude ranges. The agreement is particularly close in some cases such as in polar spring and a large fraction of the altitude range in polar summer. However, the SABER H₂O enhancement in the polar summer PMC region (>80 km) is less than expected (–15% to –20%). This will await further evaluation regarding how it will affect PMC studies.

The vertical distribution of the mean differences shows consistency in most comparisons regardless of the data set, season, and latitude range. A few critical altitudes where the sign conversion occurs are roughly at 25–30 km (positive to negative), 40–45 km (negative to positive), and 65–80 km (positive to negative), but these altitudes may shift upward or downward depending on the cases. The overall agreement between SABER and MLS H₂O is the best with the mean difference staying within ±10% in most cases. With respect to MIPAS the mean difference also stays within ±10% in most cases but we should note that MIPAS only scans up to 68 km tangent height for the nominal mode measurements and therefore comparisons above this altitude are not available. In addition, in the SABER versus ACE comparisons, the mean difference shifts slightly toward the positive direction with SABER H₂O being larger.

In the stratopause region in particular, the SABER H₂O VMRs are larger by at least ~5–10% with respect to all the other data sets used. In some cases this mean difference marginally exceeds the combined systematic error which points to a real bias. This often occurs in the comparisons with ACE H₂O. The largest mean difference (20% or greater) occurs in the SH polar winter stratopause region and below 25 km altitude with respect to all the other data sets used. In addition to this, polar fall is also the season when the mean difference in the stratopause region is generally larger. The agreement is otherwise excellent with the mean difference staying within ±10% in most cases. In polar summer specifically, the agreement below ~75 km is excellent staying within 2–5% in most cases. In the core latitude range (50°S–50°N) the mean difference is generally contained staying within ±10% but in a few cases at the lower or higher altitude limit, it reaches 20%.

The SABER and SOFIE H₂O comparisons show systematically larger mean differences which is due to the SOFIE negative biases that exist in the mesosphere. But SOFIE H₂O captures both the spatial and temporal variability exceptionally well and therefore is valuable to compare with to evaluate whether SABER H₂O effectively reflects the balance between dynamics and chemistry in the polar stratosphere and mesosphere.

Both SABER and MLS H₂O show clear day/night differences in the polar mesosphere reaching 1–2 ppmv based on the coincidence analysis which provides a new platform to study diurnal variability in H₂O. However, there is a discrepancy in the equatorial region where the SABER H₂O day/night difference remains quite significant whereas in the MLS H₂O it diminishes. This is something the future data user should be cautious about. More thorough scientific investigation is required to fully evaluate this situation.

Validation of the polar mesospheric H₂O variability is important since it exhibits drastically larger seasonal variability over the course of

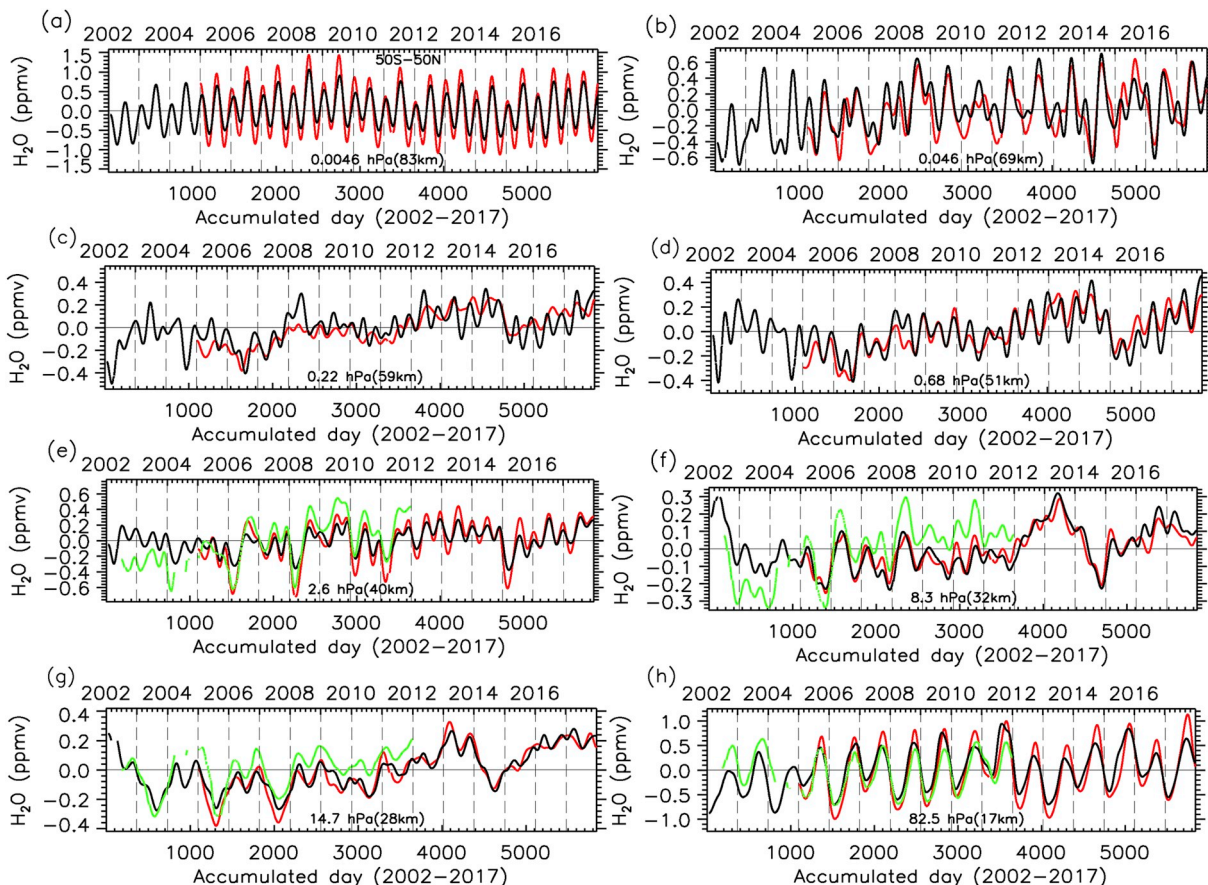


Fig. 25. SABER (black), MLS (red), and MIPAS (green) H₂O long term series at selected MLS pressure levels. For each data set at a given pressure level averaging over latitude range 50°S-50°N is carried out daily and then a 60-day smoothing is applied to the daily time series. (For interpretation of the references to color in this figure legend, the reader is referred to the Web version of this article.)

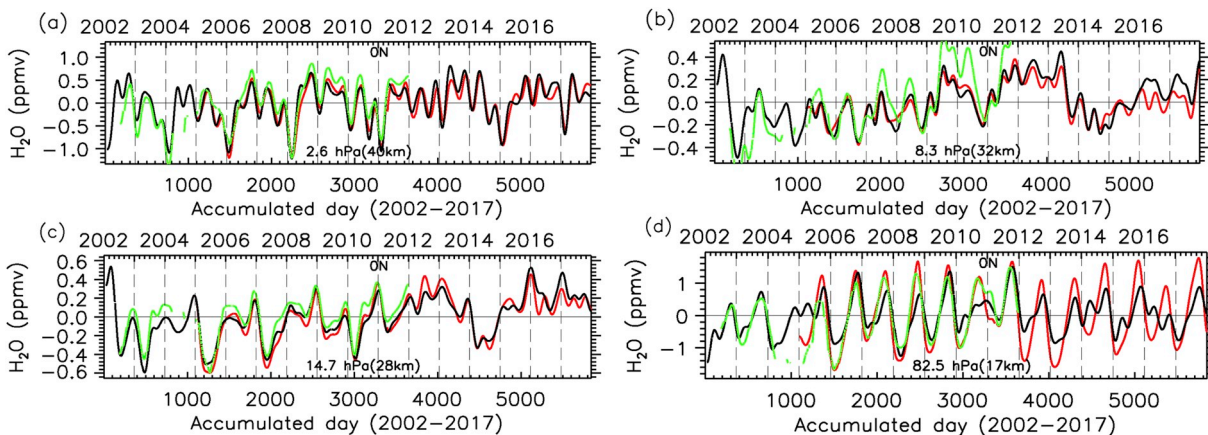


Fig. 26. Same as Fig. 25 except for a smaller latitude bin of 0°–5°N. This is to show that in a more localized latitude range, i.e., at the equator in this case, much better agreement can be achieved between SABER and MIPAS H₂O.

a year than in the middle to low latitude region. The mesospheric residual circulation drives the variability (Dunkerton, 1978; Garcia and Solomon, 1985; Garcia, 1989; Rong et al., 2016) through inducing the winter and spring descent of low H₂O VMRs and the summer ascent of the high H₂O VMRs. The alternate yaw cycles in SABER enable partial coverage of these H₂O variability modes. We have verified that the polar winter and spring descent of low H₂O VMRs, or lack of these events, are faithfully captured in SABER H₂O based on the comparisons with both SOFIE and MLS H₂O. In polar summer however, the H₂O isopleth

gradient and slope are not captured to a high precision. The polar fall isopleth gradient and slope are captured well but the stratopause peak value is larger (by ~0.8–1.6 ppmv or ~12–20%) which is also echoed in the profile comparisons.

SABER H₂O long-term time series with a 60-day smoothing applied in the core latitude range 50°S-50°N show close agreement with MLS H₂O on a series of pressure levels throughout the stratosphere and mesosphere. The agreement with MIPAS H₂O is also reasonable especially on annual to semi-annual scales, but MIPAS H₂O tends to exhibit

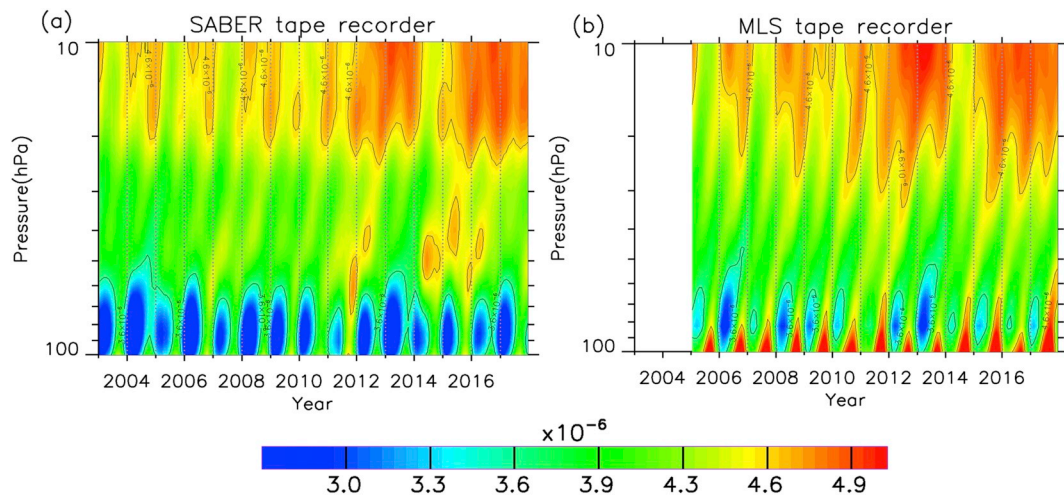


Fig. 27. The “tape recorder” features throughout the tropopause and lower stratosphere averaged over the latitude range 25°S – 25°N. (a) SABER H₂O, and (b) MLS H₂O.

stronger decadal scale variability in the lower mesosphere that is not shown in SABER H₂O. Throughout the years 2002–2005 SABER and MIPAS time series agree well at the equator which serves as an unprecedented validation over a time period when data availability is generally poor. The high degree of agreement with MLS suggests that SABER likely did not experience any systematic drift caused by data sampling or possible instrument effects over the long course of the last 17 years. The SABER H₂O “tape-recorder” features in the tropical lower stratosphere (10–100 hPa) agree well with the MLS results in terms of the variability pattern and the inter-annual and decadal variability.

Acknowledgments

This work was accomplished in the Center for Atmospheric Sciences (CAS), Hampton University in Hampton Virginia. We are grateful to the SABER retrieval team from GATS, Inc. for their tireless effort to produce the SABER v2.07 H₂O data. We acknowledge the MLS team from JPL who made MLS v4.2 available online, provided the script for the data download and made the reading routines easily accessible. We acknowledge the Scisat-1 ACE retrieval team who made their data available online for the registered users. The ACE mission is supported by the Canadian Space Agency with P. Bernath (Old Dominion University and University of Waterloo) as Mission Scientist. We also acknowledge the European Space Agency (ESA) for approving our request to use MIPAS reanalysis data and to make the corresponding error analysis available online. This work is supported under NASA contract NAG 5–11409. The H₂O data set used in this paper was obtained from the GATS-Inc ftp site at <http://saber.gats-inc.com/>. It is now released to the public and is available for download.

Appendix A. Supplementary data

Supplementary data to this article can be found online at <https://doi.org/10.1016/j.jastp.2019.105099>.

References

Bailey, S.M., Thurairajah, B., Randall, C.E., Holt, L., Harvey, V.L., Siskind, D.E., Venkataramani, K., Hervig, M.E., Rong, P., Russell III, J.M., 2014. A multi-tracer analysis of thermosphere to stratosphere descent triggered by the 2013 Stratospheric Sudden Warming. *Geophys. Res. Lett.* 41, 5216–5222. <https://doi.org/10.1002/2014GL059860>.

Bernath, P.F., et al., 2005. Atmospheric chemistry experiment (ACE): mission overview. *Geophys. Res. Lett.* 32, L15S01. <https://doi.org/10.1029/2005GL022386>.

Brasseur, G., Solomon, S., 2005. *Aeronomy of the Middle Atmosphere: Chemistry and Physics of the Stratosphere and Mesosphere*, third ed. Springer, Dordrecht, Netherlands.

Butchart, N., 2014. The Brewer-Dobson circulation. *Rev. Geophys.* 52, 157–184. <https://doi.org/10.1002/2013RG000448>.

Carleer, M.R., et al., 2008. Validation of water vapour profiles from the atmospheric chemistry experiment (ACE). *Atmos. Chem. Phys. Discuss.* 8, 4499–4559.

Cortesi, U., et al., 2007. Geophysical validation of MIPAS-ENVISAT operational ozone data. *Atmos. Chem. Phys.* 7, 4807–4867.

Dunkerton, T., 1978. On the mean meridional mass motions of the stratosphere and mesosphere. *J. Atmos. Sci.* 35, 2325–2333. [https://doi.org/10.1175/1520-0469\(1978\)035<2325:OTMMMM>2.0.CO;2](https://doi.org/10.1175/1520-0469(1978)035<2325:OTMMMM>2.0.CO;2).

Engel, A., Bönnisch, H., Schwarzenberger, T., Haase, H.-P., Grunow, K., Abalichin, J., Sala, S., 2016. Long-term validation of ESA operational retrieval (version 6.0) of MIPAS Envisat vertical profiles of methane, nitrous oxide, CFC11, and CFC12 using balloon-borne observations and trajectory matching. *Atmos. Meas. Tech.* 9, 1051–1062. <https://doi.org/10.5194/amt-9-1051-2016>.

Fischer, H., et al., 2000. ENVISAT, MIPAS: an Instrument for Atmospheric Chemistry and Climate Research ESA SP-1229. Eur. Space Agency, Noordwijk, Netherlands.

Froidevaux, L., et al., 2008. Validation of Aura microwave limb sounder stratospheric ozone measurements. *J. Geophys. Res.* 113, D15S20. <https://doi.org/10.1029/2007JD008771>.

Garcia, R.R., 1989. Dynamics, radiation, and photochemistry in the mesosphere: implications for the formation of noctilucent clouds. *J. Geophys. Res.* 94 (D12), 14,605–14,615. <https://doi.org/10.1029/JD094iD12p14605>.

Garcia, R.R., Solomon, S., 1985. The effect of breaking gravity waves on the dynamics and chemical composition of the mesosphere and lower thermosphere. *J. Geophys. Res.* 90 (D2), 3850–3868. <https://doi.org/10.1029/JD090iD02p3850>.

Gordley, L.L., Russell III, J.M., 1981. Rapid inversion of limb radiance data using an emissivity growth approximation. *Appl. Opt.* 20 (5), 807–813. <https://doi.org/10.1364/AO.20.000807>.

Gordley, L.L., et al., 2009. The solar occultation for ice experiment. *J. Atmos. Sol. Terr. Phys.* 71, 300–315. <https://doi.org/10.1016/j.jastp.2008.07.012>.

Hallgren, K., Hartogh, P., 2012. First detection of tidal behaviour in polar mesospheric water vapour by ground based microwave spectroscopy. *Atmos. Chem. Phys.* 12, 3753–3759. <https://doi.org/10.5194/acp-12-3753-2012>. www.atmos-chem-phys.net/12/3753/2012/.

Hervig, M.E., Gordley, L.L., 2010. Temperature, shape, and phase of mesospheric ice from Solar Occultation for Ice Experiment observations. *J. Geophys. Res.* 115, D15208. <https://doi.org/10.1029/2010JD013918>.

Hervig, M.E., Siskind, D.E., 2006. Decadal and inter-hemispheric variability in polar mesospheric clouds, water vapor, and temperature. *J. Atmos. Sol. Terr. Phys.* 68, 30–41. <https://doi.org/10.1016/j.jastp.2005.08.010>.

Hervig, M.E., Stevens, M.H., Gordley, L.L., Deaver, L.E., Russell III, J.M., Bailey, S.M., 2009. Relationships between PMCs, temperature and water vapor from SOFIE observations. *J. Geophys. Res.* 114, D20203. <https://doi.org/10.1029/2009JD012302>.

Lambert, A., et al., 2007. Validation of the Aura Microwave Limb Sounder middle atmosphere water vapor and nitrous oxide measurements. *J. Geophys. Res.* 112, D24S36. <https://doi.org/10.1029/2007JD008724>.

Livesey, N.J., Snyder, W.V., Read, W.G., Wagner, P.A., 2006. Retrieval algorithms for the EOS microwave limb sounder (MLS). *IEEE Trans. Geosci. Remote Sens.* 44, 1144–1155.

Lopez-Puertas, M., et al., 1995. Non-local thermodynamic equilibrium model for H₂O 6.3 and 2.7- μ m bands in the middle atmosphere. *J. Geophys. Res.* 100, 9131–9147.

Marshall, B.T., Gordley, L.L., Chu, D.A., 1994. BANDPAK algorithms for modeling broadband transmission and radiance. *J. Quant. Spectrosc. Radiat. Transfer* 52, 581–599. [https://doi.org/10.1016/0022-4073\(94\)90026-4](https://doi.org/10.1016/0022-4073(94)90026-4).

McClintock, W., Rusch, D.W., Thomas, G.E., Merkel, A.W., Lankton, M.R., Drake, V.A., Bailey, S.M., Russell III, J.M., 2009. The cloud imaging and particle size experiment on the Aeronomy of Ice in the mesosphere mission: instrument concept, design,

- calibration, and on-orbit performance. *J. Atmos. Sol. Terr. Phys.* <https://doi.org/10.1016/j.jastp.2008.10.011>.
- Mlynczak, M.G., Olander, D.S., Lopez-Puertas, M., 1994. Rapid computation of spectrally integrated nonlocal thermodynamic equilibrium limb emission. *J. Geophys. Res.* 99 (25), 772. <https://doi.org/10.1029/94JD02397>, 761 – 25.
- Mote, P.W., et al., 1996. An atmospheric tape recorder: the imprint of tropical tropopause temperatures on stratospheric water vapor. *J. Geophys. Res.* 101 (D2), 3989–4006.
- Randall, C.E., Harvey, V.L., Singleton, C.S., Bernath, P.F., Boone, C.D., Kozyra, J.U., 2006. Enhanced NO_x in 2006 linked to strong upper stratospheric Arctic vortex. *Geophys. Res. Lett.* 33, L18811. <https://doi.org/10.1029/2006GL027160>.
- Raspollini, P., et al., 2006. MIPAS level 2 operational analysis. *Atmos. Chem. Phys.* 6, 5605–5630.
- Remsberg, E.E., et al., 2008. Assessment of the quality of the Version 1.07 temperature versus pressure profiles of the middle atmosphere from TIMED/SABER. *J. Geophys. Res.* 113, D17101 <https://doi.org/10.1029/2008JD010013>.
- Remsberg, E., Damadeo, R., Natarajan, M., Bhatt, P., 2018. Observed responses of mesospheric water vapor to solar cycle and dynamical forcings. *J. Geophys. Res.* 123. <https://doi.org/10.1002/2017JD028029>.
- Rong, P., Russell III, J.M., Gordley, L., Hervig, M., Deaver, L., Siskind, D., Bernath, P., Walker, K.A., 2010. Validation of v1.022 mesospheric water vapor observed by the SOFIE instrument onboard the AIM satellite. *J. Geophys. Res.* 115, D24314. <https://doi.org/10.1029/2010JD014269>.
- Rong, P.P., Russell III, J.M., Marshall, B.T., Siskind, D.E., Hervig, M.E., Gordley, L.L., Bernath, P.F., Walker, K.A., 2016. Version 1.3 AIM SOFIE measured methane (CH₄): validation and seasonal climatology. *J. Geophys. Res. Atmos.* 121 <https://doi.org/10.1002/2016JD025415>.
- Russell III, J.M., Drayson, S.R., 1972. The inference of atmospheric ozone using satellite horizon measurements in the 1042 cm⁻¹ band. *J. Atmos. Sci.* 29, 376–390. [https://doi.org/10.1175/1520-0469\(1972\)029<0376:TIOAOU>2.0.CO;2](https://doi.org/10.1175/1520-0469(1972)029<0376:TIOAOU>2.0.CO;2).
- Russell III, J.M., Gordley, L.L., Park, J.H., Drayson, S.R., Hesketh, W.D., Cicerone, R.J., Tuck, A.F., Frederick, J.E., Harries, J.E., Crutzen, P.J., 1993. The halogen occultation experiment. *J. Geophys. Res.* 98 (D6), 10,777–10,797. <https://doi.org/10.1029/93JD00799>.
- Russell III, J.M., Mlynczak, M.G., Gordley, L.L., Tansock, J.J., Esplin, R.W., 1999. Overview of the SABER experiment and preliminary calibration results. *Proc. SPIE-Int. Soc. Opt. Eng.* 3756, 277–288.
- Russell III, J.M., et al., 2009. The Aeronomy of Ice in the Mesosphere (AIM) mission: overview and early science results. *J. Atmos. Sol. Terr. Phys.* 71 (3–4), 289–299. <https://doi.org/10.1016/j.jastp.2008.08.011>.
- Russell III, J.M., Rong, P., Hervig, M.E., Siskind, D.E., Stevens, M.H., Bailey, S.M., Gumbel, J., 2014. Analysis of northern midlatitude noctilucent cloud occurrences using satellite data and modeling. *J. Geophys. Res. Atmos.* 119, 3238–3250. <https://doi.org/10.1002/2013JD021017>.
- Siskind, D.E., et al., 2016. Persistence of upper stratospheric winter time tracer variability into the Arctic spring and summer. *Atmos. Chem. Phys. Discuss.* <https://doi.org/10.5194/acp-2015-1037>.
- Solomon, et al., 2010. Contributions of stratospheric water vapor to decadal changes in the rate of global warming. *Science* 327.
- Summers, M.E., Conway, R.R., Englert, C.R., Siskind, D.E., McHugh, M.J., Stevens, M.H., Russell III, J.M., Gordley, L.L., McHugh, M.J., 2001. Discovery of a water vapor layer in the arctic summer mesosphere: implications for polar mesospheric clouds. *Geophys. Res. Lett.* 28 (18), 3601–3604. <https://doi.org/10.1029/2001GL013217>.
- Tansock, J.J., Russell III, J.M., Mlynczak, M.G., Gordley, L.L., Brown, C., Paxton, G., McMichael, P., 2006. An update of sounding of the atmosphere using broadband emission radiometry (SABER) calibration. *Proc. SPIE Int. Soc. Opt. Eng.* 6297 <https://doi.org/10.1117/12.692857>. Infrared Spaceborne Remote Sensing XIV, 62970V (30 October 2006). <https://doi.org/10.1117/12.692857>.
- Thomas, G.E., 2003. Are noctilucent clouds harbingers of global change in the middle atmosphere? *Adv. Space Res.* 32 (9), 1737–1746. [10.1016/S0273-1177\(03\)00674-4](https://doi.org/10.1016/S0273-1177(03)00674-4).
- Waters, J.W., et al., 2006. The earth observing system microwave limb sounder (EOS MLS) on the Aura satellite. *IEEE Trans. Geosci. Remote Sens.* 44, 1075–1092.
- Wetzel, G., et al., 2013. Validation of MIPAS-ENVISAT H₂O operational data collected between July 2002 and March 2004. *Atmos. Chem. Phys.* 13, 5791–5811, 2013.